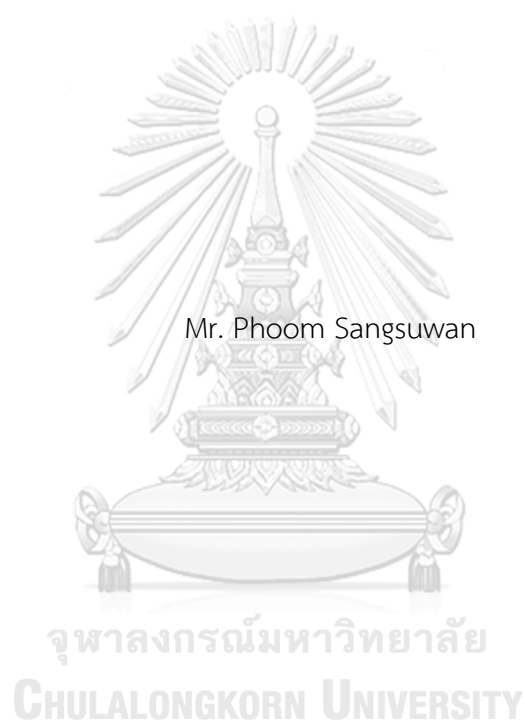


FLUORESCENT SENSORS FROM SALICYLALDIMINE DERIVATIVES FOR METAL IONS



A Thesis Submitted in Partial Fulfillment of the Requirements
for the Degree of Master of Science in Chemistry
Department of Chemistry
Faculty of Science
Chulalongkorn University
Academic Year 2018
Copyright of Chulalongkorn University

ฟลูออเรสเซนซ์เซ็นเซอร์จากอนุพันธ์ซาลิไซลัดมีนสำหรับไอออนโลหะ



วิทยานิพนธ์นี้เป็นส่วนหนึ่งของการศึกษาตามหลักสูตรปริญญาวิทยาศาสตรมหาบัณฑิต

สาขาวิชาเคมี ภาควิชาเคมี

คณะวิทยาศาสตร์ จุฬาลงกรณ์มหาวิทยาลัย

ปีการศึกษา 2561

ลิขสิทธิ์ของจุฬาลงกรณ์มหาวิทยาลัย

ภูมิ สังข์สุวรรณ : ฟลูออเรสเซนต์เซ็นเซอร์จากอนุพันธ์ซาลิไซลัลดีมีนสำหรับไอออนโลหะ. (FLUORESCENT SENSORS FROM SALICYLALDIMINE DERIVATIVES FOR METAL IONS) อ.ที่ปรึกษาหลัก : ศ. ดร.มงคล สุขวัฒนาสินิทธิ์, อ.ที่ปรึกษาร่วม : รศ. ดร.ไพฑูรย์ รัชตะสาคร

กระบวนการสังเคราะห์และตรวจวัดแบบ *in-situ* ได้ถูกพัฒนาเป็นวิธีคัดกรองฟลูออเรสเซนต์เซ็นเซอร์สำหรับไอออนโลหะที่รวดเร็ว อนุพันธ์ซาลิไซลัลดีมีน 45 ชนิดจากกระบวนการควบแน่นแบบ *in-situ* ระหว่างซาลิซาลดีไฮด์ 5 ชนิดและเอมีน 9 ชนิด ควบคู่กับซาลิซาลดีไฮด์ทั้ง 5 ชนิดในอัตรา 96 หลุมที่มีและไม่มีไอออนโลหะ 18 ชนิดถูกถ่ายภาพภายใต้แสงอัลตราไวโอเล็ต การตอบสนองของการเรืองแสงได้ถูกแปลงเป็นค่า RGB ผลการวิเคราะห์ด้วยวิธี PCA ของค่า ΔRGB ซึ่งเป็นส่วนต่างของค่าจากภาพที่มีและไม่มีไอออนโลหะพบว่าเซ็นเซอร์ 9 ชนิดมีค่า normalized loading value สูงกว่าร้อยละ 70. Sensor array ซึ่งประกอบด้วยเซ็นเซอร์ทั้ง 9 ชนิดสามารถจำแนกไอออนโลหะ 15 ชนิดนอกเหนือจากไอออนโลหะกลุ่มแอลคาไลน์ได้ด้วยความแม่นยำร้อยละ 99 จากการทดสอบครอสวาเลชันแบบ leave-one-out การครอสวาเลชันของข้อมูลจากการจัดหมู่ทุกแบบที่เป็นไปได้ของข้อมูลจากเซ็นเซอร์ตั้งแต่ 2-9 ชนิดแสดงให้เห็นว่าเซ็นเซอร์บางคู่สามารถจำแนกไอออนโลหะได้โดยไม่สูญเสียความแม่นยำ กระบวนการสังเคราะห์และตรวจวัดแบบ *in-situ* นี้ยังได้ถูกนำไปใช้เพื่อชี้ตัวเซ็นเซอร์ชนิดใหม่ที่เลือกจำเพาะกับ Al^{3+} จาก hydrazones 10 ชนิดซึ่งเกิดจากซาลิซาลดีไฮด์ 5 ชนิดและ dihydrazide 2 ชนิด อย่างไรก็ตามระยะเวลาในการตอบสนองของเซ็นเซอร์ชนิดนี้นั้นค่อนข้างช้าและยังคงต้องทำการศึกษาเพิ่มเติมเพื่อทำความเข้าใจกลไกการตรวจวัด

สาขาวิชา เคมี
ปีการศึกษา 2561

ลายมือชื่อนิสิต
ลายมือชื่อ อ.ที่ปรึกษาหลัก
ลายมือชื่อ อ.ที่ปรึกษาร่วม

5872020523 : MAJOR CHEMISTRY

KEYWORD: Principal component analysis, high-throughput screening,
salicylaldimine, Fluorescent chemosensors for metal ions

An *in-situ* forming and sensing was developed as a high-throughput screening of fluorescent chemosensors for metal ions. The 45 salicylaldimines, formed *in-situ* from the condensation between 5 salicylaldehydes and 9 amines, in 96 well-plates were photographed under black light along with the 5 salicylaldehydes in the absence and presence of 18 metal ions. The library of fluorescence response images of these 50 chemosensors were processed into RGB values. The PCA of the Δ RGB, the differences between those of images with and without the metal ions, showed 9 sensors with normalized loading value over 70%. The sensor array constructed from these 9 sensors could classify 15 non-alkali metal ions with 99% accuracy based on a leave-one-out cross-validation. The cross-validation of the data from all possible combinations of 2-9 sensors revealed that certain pairs of sensors could also classify the metal ions without any loss of accuracy. This *in-situ* forming-sensing technique was also applied to identify a new selective sensor for Al^{3+} from 10 hydrazones generated from 5 salicylaldehyde and 2 dihydrazides. However, the response time of the hydrazone sensor is relatively slow and further investigation is needed to understand the sensing mechanism.

Field of Study: Chemistry

Academic Year: 2018

Student's Signature

Advisor's Signature

Co-advisor's Signature

ACKNOWLEDGEMENTS

I would like to express my sincere gratitude to my advisor, Professor Dr. Mongkol Sukwattanasinitt, for giving me invaluable opportunities, advice, guidance, support and encouragement throughout the entire course of this research.

My sincere thanks are also extended to my co-advisor associate professor Dr. Paitoon Rashatasakhon and associate professor Dr. Kanet Wongravee for their generous guidance, advice and support.

I would like to gratefully acknowledge the committee associate professor Dr. Vudhichai Parasuk, assistant professor Dr. Thanit Praneenarat and Dr. Somboon Sahasithiwat for their kindness and valuable suggestions.

I also thank Development and Promotion of Science and Technology Talents scholarship for my financial support.

Phoom Sangsuwan



TABLE OF CONTENTS

	Page
.....	iii
ABSTRACT (THAI).....	iii
.....	iv
ABSTRACT (ENGLISH).....	iv
ACKNOWLEDGEMENTS.....	v
TABLE OF CONTENTS.....	vi
TABLE OF FIGURES.....	viii
TABLE OF TABLES.....	xi
TABLE OF SCHEMES.....	xii
LIST OF ABBREVIATIONS.....	xiii
CHAPTER I INTRODUCTION.....	1
1.1 Metal ions.....	1
1.2 Fluorescent chemosensors for metal ions.....	2
1.3 Salicylaldimine.....	4
1.4 Combinatorial approach.....	6
1.5 Multivariate statistical analysis.....	9
1.5.1 Principal component analysis (PCA).....	9
1.5.2 Linear discriminant analysis (LDA).....	10
CHAPTER II EXPERIMENT.....	13
2.1 Chemicals and materials.....	13
2.2 Analytical instruments.....	13

2.3 Screening procedures and data analysis.....	13
2.4 Synthesis	14
2.4.1 Methyl 3-formyl-2-hydroxybenzoate (s5).....	14
2.4.2 2-furancarbohydrazide (a8)	15
2.4.3 Methyl 2-pyrrolecarboxylate	15
2.4.4 2-pyrrolecarbohydrazide (a9).....	16
2.4.5 Dimethyl furan-2,5-dicarboxylate	16
2.4.6 Furan-2,5-dicarbohydrazide (a10).....	16
2.4.7 Dimethyl thiophene-2,5-dicarboxylate.....	17
2.4.8 Thiophene-2,5-dicarbohydrazide (a11).....	17
2.4.9 2-(((2-(dimethylamino)ethyl)imino)methyl)-6-methoxyphenol (s2a4).....	18
2.4.10 (N^2, N^5)- N^2, N^5 -bis(2-hydroxybenzylidene)thiophene-2,5- dicarbohydrazide-2-(((2-(dimethylamino)ethyl)imino)methyl)-6- methoxyphenol (s1a11).....	18
CHAPTER III RESULTS AND DISCUSSION	19
3.1 Synthesis	19
3.2 Metal ion sensing test of salicylaldimines.....	20
3.3 Multivariate statistical analysis.....	23
3.4 Study of dihydrazide sensors	28
CHAPTER IV CONCLUSION	35
APPENDIX.....	36
REFERENCES	41
VITA.....	44

TABLE OF FIGURES

Figure 1.1 Jabonski's diagram [3].	3
Figure 1.2 Structure of L1	4
Figure 1.3 Structure of L2	4
Figure 1.4 Structure of L3 and its complex with Zn^{2+} ion.	5
Figure 1.5 Structure of L4 and its complex with Zn^{2+} ion.	5
Figure 1.6 Structure of L5 .	6
Figure 1.7 (From left to right) Structure of L6 , L7 and L8 and their responses with Al^{3+} ion.	6
Figure 1.8 Biarylpyridine core of chemosensors.	7
Figure 1.9 Structures of a) building blocks of receptor and fluorophore b) example of bead-supported chemosensor.	8
Figure 1.10 Systematically reduction of sensors in arrays using statistical contribution from PCA.	10
Figure 1.11 LDA score plots of nine-sensors array to 10 metal ions (1mM) at pH7. ...	11
Figure 1.12 LDA score plot of fluorescent responses from 2 sensors upon mixing with each bacterial sample.	12
Figure 3.1 The photographic images of fluorescence responses of mixtures of salicylaldehydes (s1-s5 , 1 mM) and amines (a1-a9 , 1 mM) to metal ions (1 mM) under black light (365 nm).	21
Figure 3.2 1H NMR of a) mixture of 1:1 mole ratio of s2 and a4 , b) isolated s2a4 .	22
Figure 3.3 Fluorescence spectra of 10 μM of s2a4 in the presence of various metal ions (100 μM) in MeOH:water (999:1) using $\lambda_{ex} = 375$ nm.	23

Figure 3.4 Bar chart of combined loading values of ΔR , ΔG and ΔB values in the first 3 PCs of each sensor normalized to 100% for the maximum values. Red bars indicate selected imines.	25
Figure 3.5 PCA score plot of ΔR , ΔG and ΔB values from 9 selected sensors tested with 15 metal ions and Mili-Q water.	26
Figure 3.6 Plot of classification accuracy derived from LOOCV when using possible combinations of 1-9 sensors.	27
Figure 3.7 PCA score plot of ΔRGB values from s4a9 and s5a7	28
Figure 3.8 The photographic images of fluorescence responses of mixtures of salicylaldehydes (s1-s5 , 1 mM) and amines (a10 and a11 , 1 mM) to metal ions (1 mM) under black light (365 nm).	29
Figure 3.9 Fluorescence spectra of 10 μM of s1 and s1a11 in the presence of 100 μM Al^{3+} in MeOH:water (9:1) using $\lambda_{\text{ex}} = 415 \text{ nm}$	30
Figure 3.10 Fluorescence spectra of 10 μM of s1a11 in the presence of various metal ions (100 μM) in MeOH:water (9:1) using $\lambda_{\text{ex}} = 415 \text{ nm}$	31
Figure 3.11 Time-dependent fluorescence intensity of s1a11 with Al^{3+} ($\lambda_{\text{ex}} = 415 \text{ nm}$), inset: Fluorescence intensity at 499 nm over time.	32
Figure 3.12 ^1H NMR spectrum of s1a11 in DMSO- d_6	33
Figure 3.13 ^1H NMR titration of s1a11 and $\text{Al}_2(\text{SO}_4)_3$ in DMSO.	34
Figure A 1 ^1H NMR spectrum of Methyl 2-pyrrolicarboxylate in CDCl_3	37
Figure A 2 ^1H NMR spectrum of compound a9 in DMSO- d_6	37
Figure A 3 ^1H NMR spectrum of compound s2a4 in CDCl_3	38
Figure A 4 ^1H NMR spectrum of compound a10 in DMSO- d_6	38
Figure A 5 ^1H NMR spectrum of compound s2a4 in CDCl_3	39
Figure A 6 ^1H NMR spectrum of compound a11 in DMSO- d_6	39

Figure A 7 ^1H NMR spectrum of compound **a8** in DMSO-d₆ 40



TABLE OF TABLES

Table 1.1 EPA Regulation of hazardous metal ions in drinking water	1
Table 1.2 WHO recommended mineral intake	2



TABLE OF SCHEMES

Scheme 3.1 Synthesis of s5 , a8 and a9	19
Scheme 3.2 Structures of salicylaldehydes and amines.....	20
Scheme 3.3 Synthesis of a10 and a11	29



LIST OF ABBREVIATIONS

A	acceptor
ACN	Acetonitrile
calc.	calculated
^{13}C NMR	carbon-13 nuclear magnetic resonance
CDCl_3	deuterated chloroform
CV	Cross-validation
D	donor
d	doublet (NMR)
dd	doublet of doublet (NMR)
DBU	1,8-Diazabicycloundec-7-ene
DMSO	Dimethyl sulfoxide
DMSO-d_6	Deuterated dimethyl sulfoxide (6 D)
eq.	equivalent (s)
EtOH	Ethanol
g	gram (s)
h	hour (s)
$^1\text{H-NMR}$	proton nuclear magnetic resonance
Hz	hertz
ICT	intramolecular charged transfer
LDA	Linear discriminant analysis
LOO	Leave-one-out
m	multiplet (NMR)
M	molar

Me	methyl
MeOH	Methanol
MHz	megahertz
mg	milligram (s)
min	minute (s)
mL	milliliter (s)
mmol	millimole (s)
nm	nanometer
nM	nanomolar
OMe	methoxy
PC	Principal component
PCA	Principal component analysis
ppm	part per million
RT	room temperature
s	singlet (NMR)
<i>t</i>	tertiary
t	triplet (NMR)
UV	ultraviolet
δ	chemical shift
°C	degree Celsius
μL	microliter (s)
μM	micromolar (s)
% yield	percentage yield

CHAPTER I

INTRODUCTION

1.1 Metal ions

Non-alkali metal ions are ubiquitous in our everyday life. Some of them are essential such as Ca^{2+} , Mg^{2+} and Zn^{2+} while the others such as Hg^{2+} , Cd^{2+} and Pb^{2+} are highly toxic. Excess ingestion of many metal ions can lead to detrimental effects on health, in short-term and/or long-term. There are regulations for maximum concentration allowed in drinking water (Table 1.1) or recommended concentration in drinking water (Table 1.2) [1, 2].

Table 1.1 EPA Regulation of hazardous metal ions in drinking water

Metal ion	Regulated concentration (mg/L)	Effects on health
Hg^{2+}	<0.002	Overexposure lead to abdominal pain, vomiting, bloody diarrhea, kidney damage and death
Cd^{2+}	<0.005	Overexposure lead to kidneys problems and weaker bone
Pb^{2+}	<0.015	Overexposure lead to damage to kidneys, cardiovascular or nervous systems, impaired development in children and infants.
Al^{3+}	<0.2	Overexposure lead to impair central nervous system and Alzheimer's disease.

Table 1.2 WHO recommended mineral intake

Metal ion	Recommended intake	Biological role
Ca ²⁺	>520 mg	Key-components of bone tissues and hormonal signaling systems.
Mg ²⁺	3.5-4.0 mg per kilogram of body mass	Cofactor for many enzymes and essential in maintenance of biological electrical potential.
Zn ²⁺	1.4 mg/day	Cofactor in numerous enzymes and play crucial role in genetic expression, cell maintenance and immunity.

In daily life, human body can be exposed to metal ions by various pathways, including food and water consumption, contamination in environments, using of products containing metal ions and occupational hazards. Causes of contamination are natural and man-made. Not only human health, these metal ions also have effect on other organisms and ecosystems. Therefore, methods for detecting, identifying, measuring and controlling of metal ion concentrations are important. As metal ions are present everywhere, it is ideal to have simple and cost-effective methods. Among many methods for metal ions detection, fluorescence spectroscopy was chosen for this work.

1.2 Fluorescent chemosensors for metal ions

Fluorescence phenomenon is a radiative decay process that the excited molecule emits its excess energy in form of light. This process is involved light absorption and emission explained with Jabonski's diagram (Figure 1.1) [3]. Upon the absorption of a photon, the molecule is excited from ground state (S₀) to excited states (S₁ or S₂). The excited molecule rapidly relaxes to the lowest vibrational level of S₁ via internal conversion process. Finally, the molecule returns to ground state

with emission of a longer wavelength photon. This process occurs in nano-second timescales.

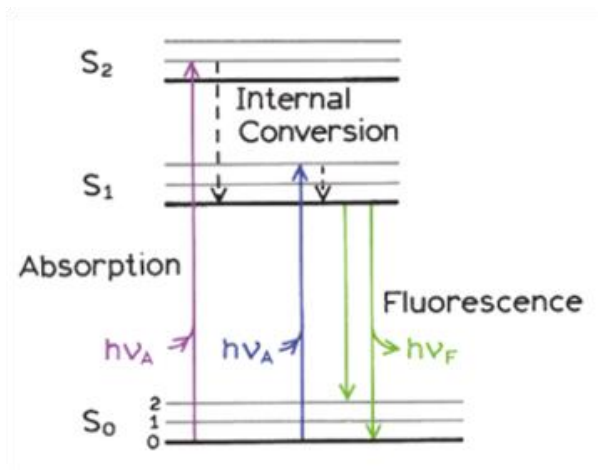


Figure 1.1 Jabonski's diagram [3].

By measuring intensity of the fluorescence emission at specific wavelength, concentration of light-emitting molecule can be determined. This is a basis of fluorometry which monitor change in fluorescence intensity of fluorescent chemosensor to measure concentration of a specific analyte, as concentration of the analyte will proportionally affect the degree of changes in chemosensor. This method held significant advantages over other methods such as high selectivity and sensitivity, cost-efficiency and simple operation. This technique also allows visualization of the result, and adaptable with a common equipment like camera, which increase its potential in on-field applications.

Most of the fluorescent chemosensors consist of two main units. A receptor unit is for selective detection of the analytes by mean of binding or chemical reaction. Another is a signaling unit, called fluorophore, which provides change in fluorescence upon detection of analyte by the receptor unit. The changes in fluorescence of chemosensors can be either increasing (turn-on) or decreasing (turn-off) of intensity or emerging of new emission peak at different wavelength (ratiometric).

1.3 Salicylaldimine

Salicylaldimines, imine derivatives of salicylaldehyde, have been used as fluorescent chemosensors for metal ions, contributed from their abilities in binding with metal ions that induce various processes effecting their fluorescence, including photo-induced electron transfer (PET), *cis-trans* isomerization, intramolecular charge transfer (ICT) and excited-state intramolecular photon transfer (ESIPT).

In 2013, Chen *et al.* [4] synthesized salicylaldimine (**L1**) from salicylaldehyde and 2-(2-aminophenoxy)ethanol (Figure 1.2). This salicylaldimine formed 1:1 complex with Al^{3+} ion in water/ethanol (5:95) solution that enhanced the fluorescence signal at 480 nm to 250 times. The limit of detection (LOD) of this chemosensor is 8.87×10^{-7} M with some quenching interference of Fe^{3+} ion.

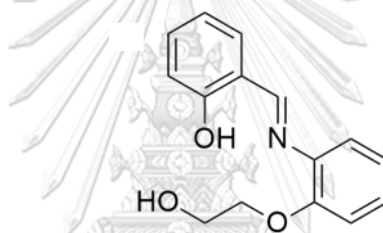


Figure 1.2 Structure of **L1**

In 2014, Chen *et al.* [5] synthesized salicylaldimine (**L2**) from 2-hydroxynaphthaldehyde and cysteamine. (Figure 1.3) This salicylaldimine can enhance fluorescence signal at 454 nm to 53 times when in presence of Al^{3+} ion in DMSO/water (40:60, v/v) solution. The salicylaldimine has LOD of 1.02×10^{-6} M with some quenching interference of Fe^{3+} and Cu^{2+} ions.

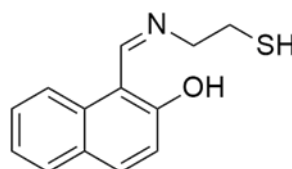


Figure 1.3 Structure of **L2**

In 2015, Pradhan *et al.* [6] synthesized salicylaldimine derivative (**L3**) of *o*-vanillin and 8-aminoquinoline, which is receptor for Zn^{2+} ion. **L3** emits fluorescence at 576 nm in acetonitrile/water (90:10, v/v) mixture. Upon binding with Zn^{2+} ion to form a 2:1

complex (Figure 1.4), the emission shifted to 595 nm and the fluorescence quantum yield increased from 0.0156 to 0.2645 due to inhibition of PET process in **L3**. This chemosensor has LOD of 130 nM with slight interference of Cd^{2+} ion.

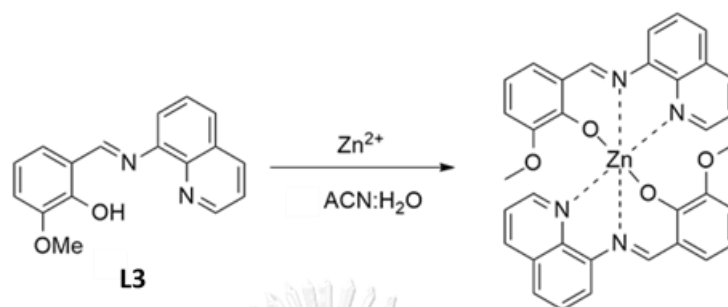


Figure 1.4 Structure of **L3** and its complex with Zn^{2+} ion.

In 2015, Sarkar *et al.* [7] synthesized salicylaldehyde derivative (**L4**) of 3,5-dichlorosalicylaldehyde and 8-aminoquinoline for Zn^{2+} ion detection in acetonitrile-water (50-50) solution mixture (Figure 1.5) Upon addition of Zn^{2+} ion fluorescence of **L4** was shifted from 563 nm to 553 nm and quantum yield of the process was increased from 0.004 to 0.143. Authors suggested that the enhancement is a result from inhibition of ESIP process, as same enhancement was observed at pH below 5. At this pH, imine moiety was protonated into iminium form and can no longer receive proton from phenol group. Complex of **L4**- Zn^{2+} ion was determined to be 2:1 complex. The limit of detection (LOD) is 5 nM. This chemosensor was interfered by Al^{3+} , Cd^{2+} and Cu^{2+} ion.

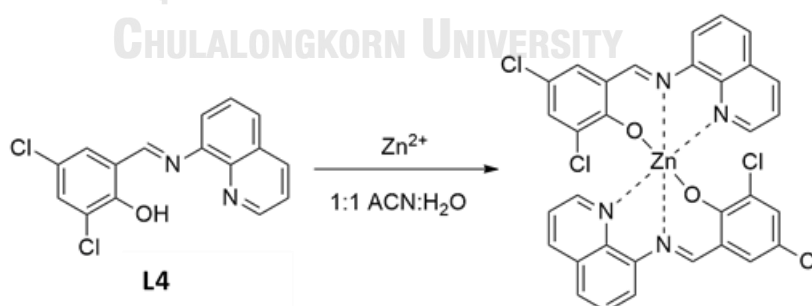


Figure 1.5 Structure of **L4** and its complex with Zn^{2+} ion.

In 2016, Saleh *et al.* [8] synthesized salicylaldehyde derivative (**L5**) from *o*-vanillin. (Figure 1.6) **L5** responds with Ca^{2+} ion in HEPES pH 7.2 buffer solution. In presence of with Ca^{2+} ion, emission intensity of **L5** signal at 545 nm was reduced and new signal at 483 nm was enhanced. Authors suggested that binding with Ca^{2+} ion

reduced electron density in **L5** and inhibit intramolecular charge transfer (ICT) process, resulting in shorter wavelength emission. **L5** has LOD of 0.3 μM and was interfered by Ba^{2+} ion.

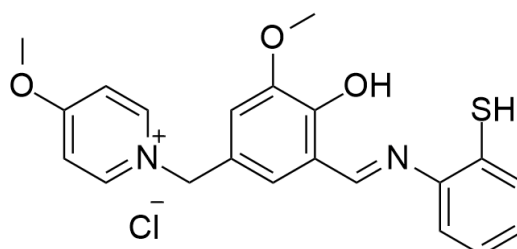


Figure 1.6 Structure of **L5**.

In 2016, Boonkitpatarakul et al. [9] synthesized a series of bis-hydrazone compounds from salicylaldehyde derivatives and furoic hydrazone (**L6-L8**) which exhibit selective fluorescence enhancement in presence of Al^{3+} ion. Binding with Al^{3+} ion inhibit PET and ESIPT process of fluorophore and resulted in large enhancement and stoke shift of fluorescence. (Figure 1.7) The selected sensor, **L8** has limit of detection of 3.1 nM in HEPES buffered aqueous solution pH 5.5.

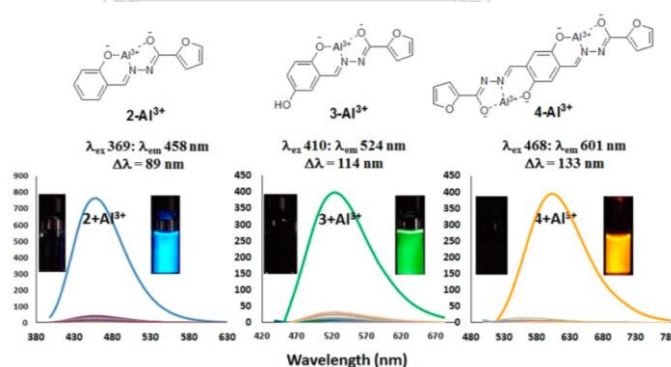


Figure 1.7 (From left to right) Structure of **L6**, **L7** and **L8** and their responses with Al^{3+} ion.

1.4 Combinatorial approach

Due to the strategy for designing a fluorescence chemosensor by combining a receptor unit and a signaling unit into a single molecule, there are numerous potential candidate structures for chemosensors. However, to rational select a pair of receptor unit and signaling unit that would perfectly combine into an excellent chemosensors

is practically impossible task. Therefore, detailed experiments for each candidate would require tremendous amount of time and resources. [10]

Fortunately, advances in synthesis bring useful tools that could be utilized in linking building blocks of chemosensors together, leading to parallel synthesis of large arrays from multiple building block. These advancements is a result from development in high-throughput experimentation, which increase demands for vast number of materials for screening. [10] By using these methods, many approaches for designing chemosensors had been developed.

In 2004, Mello and Finney [11] utilized peptide synthesis on resin bead to create a library of fluorescent chemosensors candidates for metal ions by linking various amino acid and acyl end-cap with a biarylpyridine derivative. They demonstrated that their approach identified a chemosensors for Hg^{2+} ion with $K_{\text{assoc}} = 1.8 \times 10^{-6} \text{ M}^{-1}$ in acetonitrile (Figure 1.8).

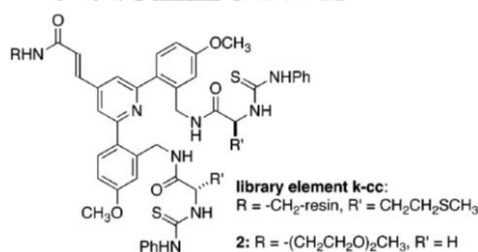


Figure 1.8 Biarylpyridine core of chemosensors.

In 2014, Yuen et al. [12] applied solid-supported nucleotide synthesis to link multiple building blocks of receptor and fluorophore together into DNA-like chemosensors (Figure 1.9). Fluorescence response images of synthesized chemosensors supported on beads were recorded and compared with images before addition of metal ions to create a large library of ΔRGB values of beads. Then they applied statistically analysis to discriminate up to 57 metal ions with 9 sensors.

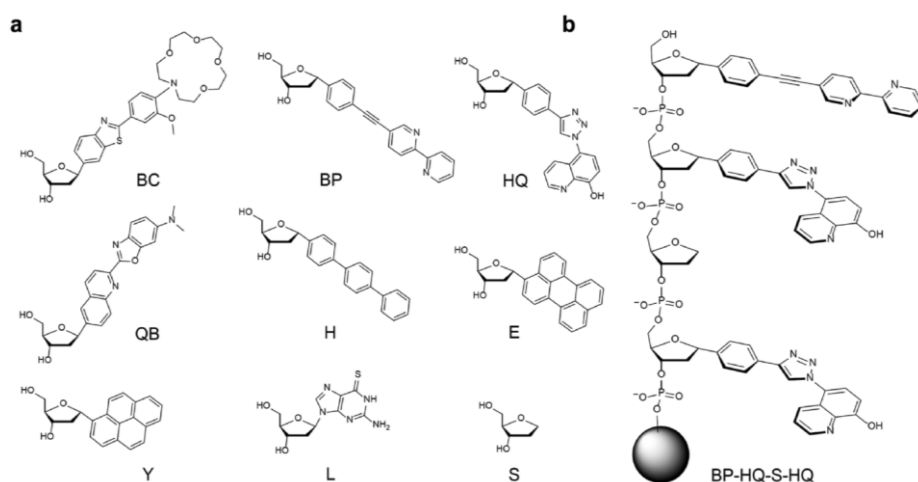


Figure 1.9 Structures of a) building blocks of receptor and fluorophore b) example of bead-supported chemosensor.

These combinatorial approach shows potentials for rapid screening of chemosensors candidates. To improve this approach, simultaneous synthesis can be applied to further increase the throughput of screening by using chemical reaction with non-interfering byproducts to generate candidates *in situ*. Formation of salicylaldehyde, which is simultaneous at room temperature and have only a water molecule as byproduct, fit perfectly to these conditions. [13]

1.5 Multivariate statistical analysis

A chemical analysis may be involved multiple variables; for an example, a single spectrum contains a pattern of data similar to a fingerprint that requires skillful and experienced chemists to interpret. For unknown samples, the analysis can involve multiple measurements, resulted in overwhelming amount of data for manual interpretation. Advancement in mathematic methods and computing technology gave birth to a way to process large amount of data and correlate them to extract meaningful information, such as pattern recognition analysis. These methods allow faster and more effective chemical analysis with many measurements and samples. Pattern recognitions of multi-dimensional data may apply multivariate statistical analysis which can be divided into two categories: 1) unsupervised methods such as principal component analysis (PCA), input the data of each sample without a predefined class, and 2) supervised methods such as linear discriminant analysis (LDA), input the data of each sample as a predefined class.

1.5.1 Principal component analysis (PCA)

One of the most wide-spread unsupervised multivariate statistical analysis is principal component analysis (PCA). The PCA transforms the data with n-dimension into scores of n orthogonal principal components (PCs). The first PC contains the highest variance of the data and other PCs contain remaining variance in decreasing order. Therefore, the first few PCs contains most of information of data distribution. This allows PCA to be used as a tool for dimensionality reduction, feature extraction and data visualization. The PCA also provide information about the statistical contribution of each original dimension, generally called loading, in each PC.

In 2008, Palacios *et al.* [14] developed sensor arrays based on 6 hydroxyquinoline-based fluorescent chemosensors for metal ions. The PCA was applied to YGB color values from photographic images to identify metal ions. Using PCA loading, the six-sensor array was reduced to two-sensor array. The resulted 2 sensors array could discriminate 10 metal ions with 100% accuracy from LDA cross-validation (Figure 1.10).

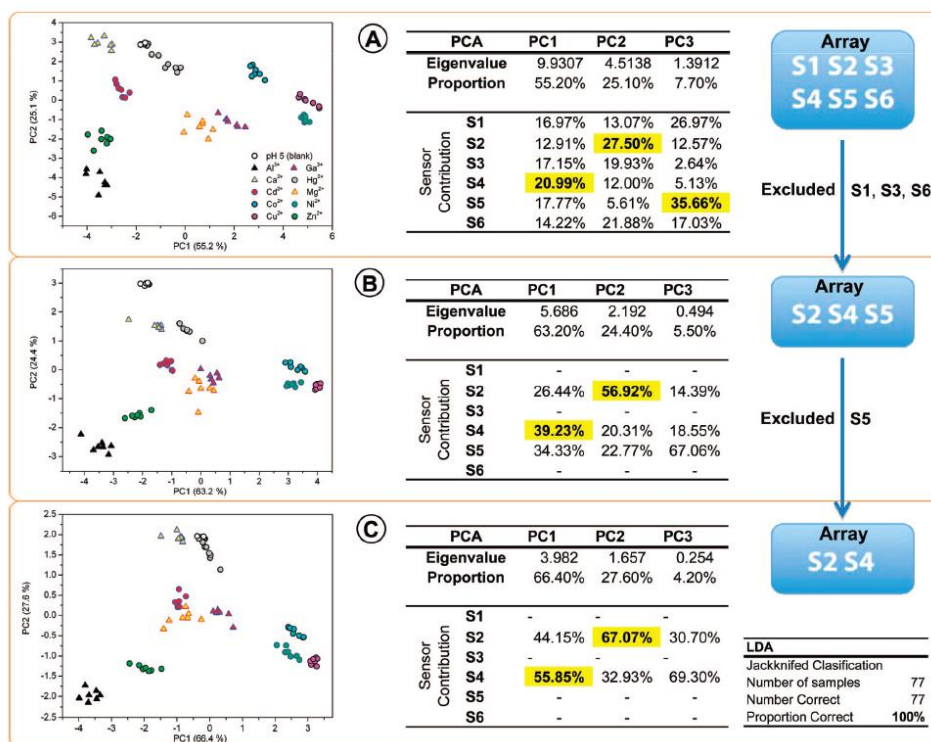


Figure 1.10 Systematically reduction of sensors in arrays using statistical contribution from PCA.

1.5.2 Linear discriminant analysis (LDA)

LDA is a supervised method, which predefine the samples into classes. The LDA also transforms the data with n-dimension into scores of n new orthogonal dimensions. Since the data were assigned into classes, the transformation tries to model the score based on the similarities among the data in the same class while generate a linear discriminant (LD) function to describe the best parameters to discriminate different class. This is achieved by maximize ratio of inter-class variance and minimize ratio of intra-class variance. Since PCA utilizes the variance in the original data for the transformation, it gives loadings that related to the contribution of the original dimension. LDA however aims to minimize the distance between samples in the same class and maximize separation among different classes, the loadings obtained from LDA does not directly related to the contribution of the original dimension.

In 2008, Wang *et al.* [15] used array of 9 fluorescent chemosensors to identify 10 metal ions at different range of pH. Photographic images of fluorescence responses

were recorded in 4 color channel (RYGB). LDA score plot of the color values from the photographic array could identify the metal ions at 5 concentrations in the range of 5-5000 μM with 96% accuracy (Figure 1.11).

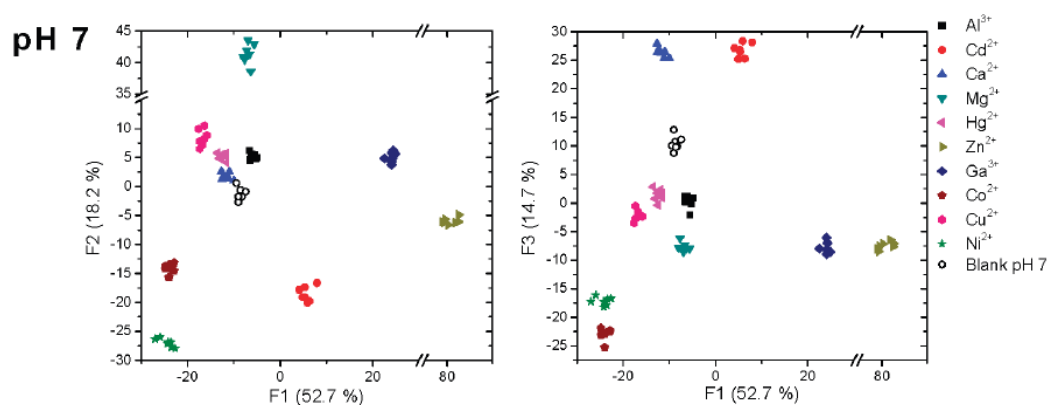


Figure 1.11 LDA score plots of nine-sensors array to 10 metal ions (1mM) at pH7.

In 2015, Mungkarndee *et al.* [16] used 3 triphenylamine-based fluorescent sensors for detection and identification of foodborne pathogens. LDA was applied to the fluorescence intensities at various wavelength in the range of 400-700 nm. The LDA loadings could exclude a low performance sensor to give a two-sensors array for identifying 8 bacteria with 100% accuracy (Figure 1.12).

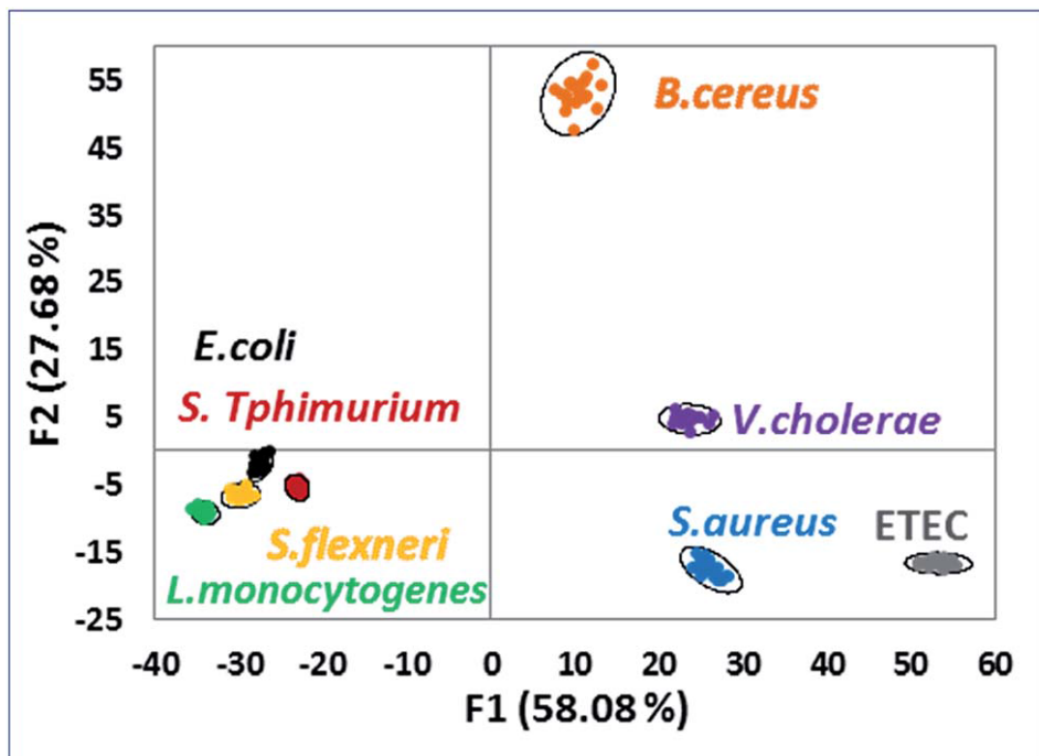


Figure 1.12 LDA score plot of fluorescent responses from 2 sensors upon mixing with each bacterial sample.

CHAPTER II

EXPERIMENT

2.1 Chemicals and materials

All chemicals were purchased from commercial suppliers (Sigma-Aldrich, Fluka, Acros, TCI or Merck) and were used without further purification. All chemicals were used as received without further purification. In analytical experiments, HPLC grade solvents (methanol and DMSO) and Milli-Q water were used. All column chromatography was carried out using Merck silica gel 60 (70-230 mesh). Thin layer chromatography (TLC) was performed on silica gel plates (Merck F245).

2.2 Analytical instruments

^1H NMR spectra were acquired on a Varian Mercury NMR spectrometer at 400 MHz and ^{13}C NMR spectra were obtained from a Bruker NMR spectrometer at 100 MHz. Absorption spectra were collected with a Varian Cary 50 UV-vis spectrophotometer. Fluorescence spectra were collected with a Varian Cary Eclipse spectrofluorometer. The absorption and emission spectra were acquired from solution in a quartz cuvette with 1 cm path length. Photographic images of well-plate are recorded using a Panasonic LUMIX Compact System (Mirrorless) Camera DMC-GF7.

2.3 Screening procedures and data analysis.

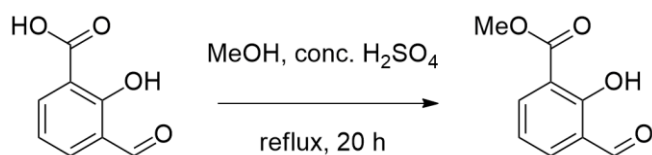
Salicylaldehyde derivatives and amines were dissolved in methanol to prepare 10 mM stock solution, with exception of two hydrazides which were dissolved in DMSO instead. Guanidine hydrochloride and methyl glycine ester hydrochloride were neutralized by addition of 0.5 equivalents of K_2CO_3 . Each stock solution of the metal ion (Li^+ , Na^+ , K^+ , Mg^{2+} , Ca^{2+} , Ba^{2+} , Al^{3+} , Fe^{2+} , Fe^{3+} , Cr^{3+} , Co^{2+} , Ni^{2+} , Cu^{2+} , Zn^{2+} , Ag^+ , Cd^{2+} , Hg^{2+} and Pb^{2+}) was prepared from the solid nitrate salt (with exceptions of $\text{Fe}(\text{CH}_3\text{COO})_2$ and $\text{Hg}(\text{CH}_3\text{COO})_2$) dissolved in Milli-Q water and diluted to 10 mM.

The sensor screening experiments were performed in a black 96-well plate. Each well consists of 140 μL of methanol as solvent and 20 μL each of aldehyde, amine and analyte stock solution (total 200 μL) and Milli-Q water was used as a blank for negative control. After the addition of the final component, the well plate was mildly shaken and rested for 10 minutes in dark place before placed in black box under four 6W 365 nm black light lamp. Photographic images of well-plate are recorded using a Panasonic LUMIX Compact System (Mirrorless) Camera DMC-GF7. Each experiment was record 2 times and the final RGB values were averaged from both images. NIH ImageJ processing software was used to determine mean R, G and B values parameters from 7,860 pixels circular selection of each well image. R, G and B values were converted into ΔR , ΔG and ΔB by subtracting the average R, G and B values of the sample with the average R, G and B values of Milli-Q water.

Multivariate data analysis such as PCA and LDA with cross-validation were performed using MATLAB R2018a program. In case of PCA, all input data set were mean-centered prior subjected to PCA analysis. The underlying variations of the sensors induced using the score of PCs. To evaluate the efficiency of sensor to predict the ion species, the predictive model was generated by using LDA with Leave-one-out cross validation approach.

2.4 Synthesis

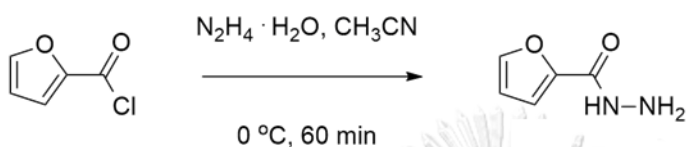
2.4.1 Methyl 3-formyl-2-hydroxylbenzoate (s5)



3-formyl-2-hydroxylbenzoate (500 mg, 3.0 mmol) was added to a sealed tube and dissolved in 1,2-dichloroethane (10 mL) and methanol (5 mL). Concentrated sulfuric acid (0.5 mL) was added and solution was refluxed for 20 hours. After cooled down, the solution was concentrated under reduced pressure and neutralized with saturated NaHCO₃ solution. The mixture was extracted with dichloromethane (3 x 10 mL). The organic layers were combined and dried over anhydrous sodium sulfate,

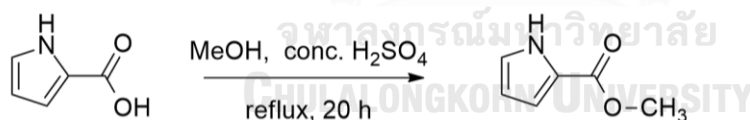
concentrated under reduced pressure and purified by column chromatography (20% ethyl acetate/hexane). The solvent was removed under reduced pressure to give 448 mg of the desired product as a yellow solid (83% yield). $^1\text{H NMR}$ (400 MHz, CDCl_3): δ (ppm) 11.54 (1H, s); 10.52 (1H, s); 8.13-8.11 (1H, dd); 8.05-8.03 (1H, dd); 7.04-7.02 (1H, t); 4.02 (3H, s).

2.4.2 2-furancarbohydrazide (a8)

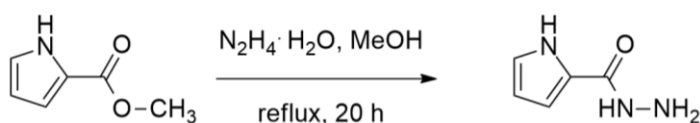


A round bottom flask was charged with hydrazide monohydrate (2 g, 40 mmol) and placed in ice bath. Solution of 2-furancarboxyl chloride (1.2 g, 9 mmol) in acetonitrile (5 mL) was added slowly under constant stirring. After 30 minutes, ice bath was removed, and the mixture was stirred for another 30 minutes. The precipitated solid was filtered, washed with cold methanol and recrystallized in ethyl acetate to give 381 mg of the desired product as a white solid. $^1\text{H NMR}$ (400 MHz, DMSO-d_6): δ (ppm) 10.28 (1H, s); 7.84 (1H, d); 7.21 (1H, d); 6.68 (1H, t).

2.4.3 Methyl 2-pyrrolicarboxylate

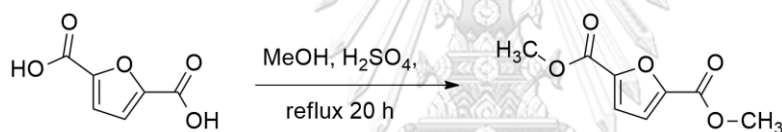


Pyrroic acid (330 mg, 3.0 mmol) was added to a round bottom flask and dissolved in methanol (20 mL). Concentrated sulfuric acid (0.5 mL) was added and the solution was refluxed for 20 hours. After cooled down, the solvent was removed under reduced pressure and pH was adjusted to slightly basic with saturated NaHCO_3 solution. The mixture was extracted with dichloromethane (3 x 10 mL). The organic layers were combined and dried over anhydrous sodium sulfate. The solvent was removed under reduced pressure to give 245 mg of the desired product as a brown solid (65% yield). $^1\text{H NMR}$ (400 MHz, CDCl_3): δ (ppm) 6.96 (1H, s); 6.92 (1H, s); 6.27 (1H, s); 3.85 (3H, s).

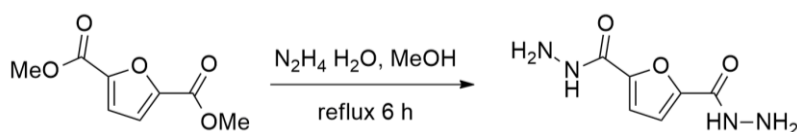
2.4.4 2-pyrrolocarbohydrazide (**a9**)

Methyl 2-pyrrolocarboxylate (240 mg, 1.9 mmol) was added to a round bottom flask and dissolved in methanol (20 mL). Hydrazide monohydrate (1 mL) was added and the solution was refluxed for 20 hours. After cooled down, the solution was concentrated under reduced pressure and precipitated solid was filtered. The solid was recrystallized in water/ethanol to give 108 mg of the desired product as a pale brown solid (45% yield). ^1H NMR (400 MHz, DMSO-d_6): δ (ppm) 11.42 (1H, s); 9.23 (1H, s); 6.86 (1H, d); 6.74 (1H, d); 6.04 (1H, t); 4.31 (2H, s).

2.4.5 Dimethyl furan-2,5-dicarboxylate

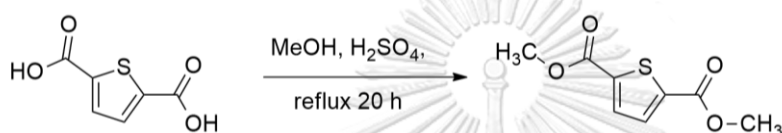


Furan-2,5-dicarboxylic acid (400 mg, 2.57 mmol) was added to a round bottom flask and dissolved in methanol (20 mL). Concentrated sulfuric acid (0.5 mL) was added and the solution was refluxed for 36 hours. After cooled down, the solvent was removed under reduced pressure and pH was adjusted to slightly basic with saturated NaHCO_3 solution. The mixture was extracted with dichloromethane (3 x 10 mL). The organic layers were combined and dried over anhydrous sodium sulfate. The solvent was removed under reduced pressure to give 260 mg of the desired product as a brown solid (55% yield). ^1H NMR (400 MHz, CDCl_3): δ (ppm) 7.24 (2H, s); 3.88 (6H, s).

2.4.6 Furan-2,5-dicarbohydrazide (**a10**)

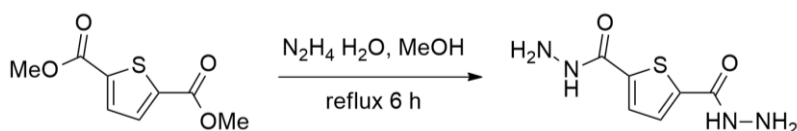
Dimethyl furan-2,5-dicarboxylate (260 mg, 1.4 mmol) was added to a round bottom flask and dissolved in methanol (10 mL). Hydrazide monohydrate (1 mL) was added and the solution was refluxed for 30 hours. After cooled down, the solution was concentrated under reduced pressure and precipitated solid was filtered. The solid was recrystallized in ethanol to give 144 mg of the desired product as a white solid (56% yield). ^1H NMR (400 MHz, DMSO- d_6): δ (ppm) 9.74 (2H, s); 7.08 (2H, s); 4.52 (4H, s).

2.4.7 Dimethyl thiophene-2,5-dicarboxylate



Thiophene-2,5-dicarboxylic acid (500 mg, 2.9 mmol) was added to a round bottom flask and dissolved in methanol (10 mL). Concentrated sulfuric acid (0.5 mL) was added and solution was refluxed for 36 hours. After cooled down, the solvent was removed under reduced pressure and pH was adjusted to slightly basic with saturated NaHCO_3 solution. The mixture was extracted with dichloromethane (3 x 10 mL). The organic layers were combined and dried over anhydrous sodium sulfate. The solvent was removed under reduced pressure to give 524 mg of the desired product as a white solid (90% yield). ^1H NMR (400 MHz, CDCl_3): δ (ppm) 7.73 (2H, s); 3.91 (6H, s).

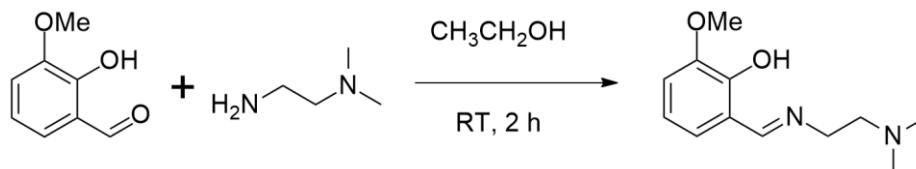
2.4.8 Thiophene-2,5-dicarbohydrazide (**a11**)



Dimethyl thiophene-2,5-dicarboxylate (500 mg, 2.5 mmol) was added to a round bottom flask and dissolved in methanol (15 mL). Hydrazide monohydrate (0.5 mL) was added and solution was refluxed for 20 hours. After cooled down, the solution was concentrated under reduced pressure and precipitated solid was filtered. The solid was recrystallized in ethanol to give 325 mg of the desired product as a white solid

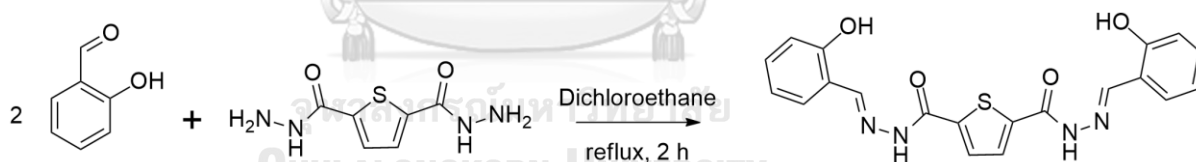
(65% yield). ^1H NMR (400 MHz, DMSO- d_6): δ (ppm) 9.88 (2H, s); 7.61 (2H, s); 4.49 (4H, s).

2.4.9 2-(((2-(dimethylamino)ethyl)imino)methyl)-6-methoxyphenol (**s2a4**)



To a solution of *o*-vanilin (**s2**) (304 mg, 2 mmol) in ethanol (10 mL), a 0.1 M solution of *N,N*-dimethylethylenediamine (**a4**) in ethanol (20 mL, 2 mmol) was added. The solution mixture was stirred at room temperature for 2 hours. The solvent was removed under reduced pressure and the liquid residue was dried under vacuum. The desired product was obtained as a yellow liquid (896 mg, quantitative yield). ^1H NMR (400 MHz, CDCl_3): δ (ppm) 8.36 (H, s); 6.89 (2H, m); 6.82 (1H, t); 3.91 (3H, s); 3.74 (2H, t); 2.66 (2H, t); 2.31 (6H, s).

2.4.10 (N^2,N^5)- N^2,N^5 -bis(2-hydroxybenzylidene)thiophene-2,5-dicarbohydrazide-2-(((2-(dimethylamino)ethyl)imino)methyl)-6-methoxyphenol (**s1a11**)



To a solution of salicylaldehyde (**s1**) (784 mg, 6.42 mmol) in 1,2-dichloroethane (30 mL), a 0.1 M solution of thiophene-2,5-dicarbohydrazide (**a11**) in 1,2-dichloroethane (30 mL, 3 mmol) was added. The solution mixture was refluxed for 2 hours. After cooled down, the precipitated solid was filtered and washed thoroughly with cold methanol. After dried under reduced pressure, the desired product was obtained as a yellow solid (1.2 g, quantitative yield). ^1H NMR (400 MHz, DMSO- d_6): δ (ppm) set 1: 12.29 (1H, s); 11.05 (1H, d); 8.67 (1H, s); 7.95 (1H, m); 7.60 (1H, d); 7.36 (1H, t); 6.90 (1H, m). set 2: 11.97 (1H, s); 10.15 (1H, d); 8.50 (1H, s); 8.05 (1H, d); 7.95 (1H, m); 7.36 (1H, t); 6.90 (1H, m).

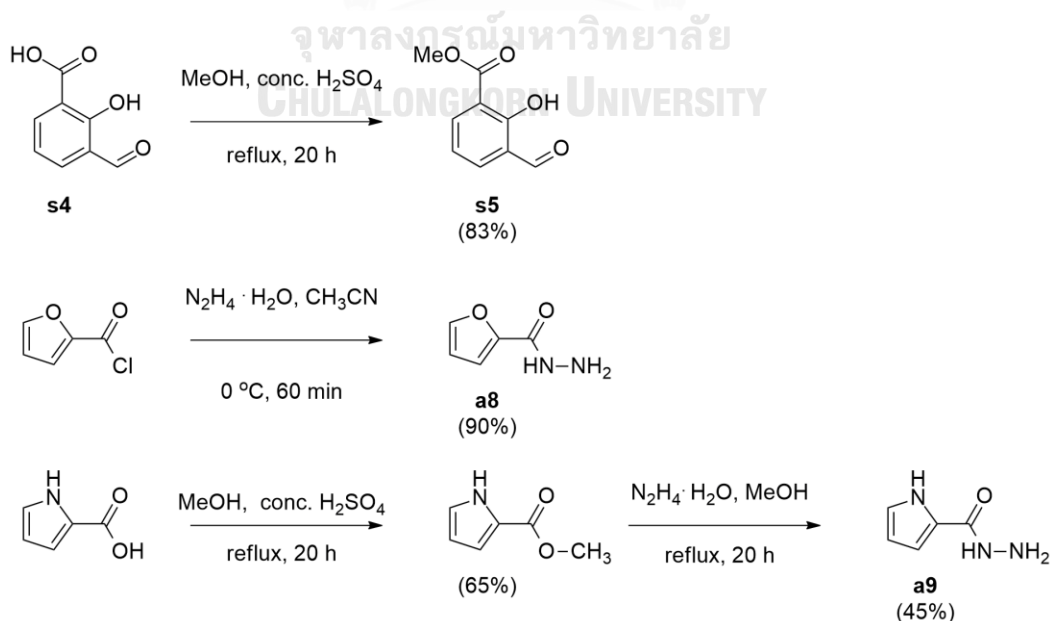
CHAPTER III

RESULTS AND DISCUSSION

In this thesis work, 45 salicylaldehydes were screened as a sensor array for metal ions. The salicylaldehydes were prepared *in-situ* from the condensation between a salicylaldehyde (**s1-s5**) and an amine (**a1-a9**). Salicylaldehydes **s1-s4** and amines **a1-a7** were commercially available. Therefore, only salicylaldehyde **s5** and amines **a8** and **a9** were synthesized. In addition, 2 dihydrazides (**a10** and **a11**) were synthesized and tested with metal ions. The results and discussion will be divided in 4 parts: synthesis, metal ion sensing test of salicylaldehydes, multivariate statistical analysis and study of dihydrazide sensors

3.1 Synthesis

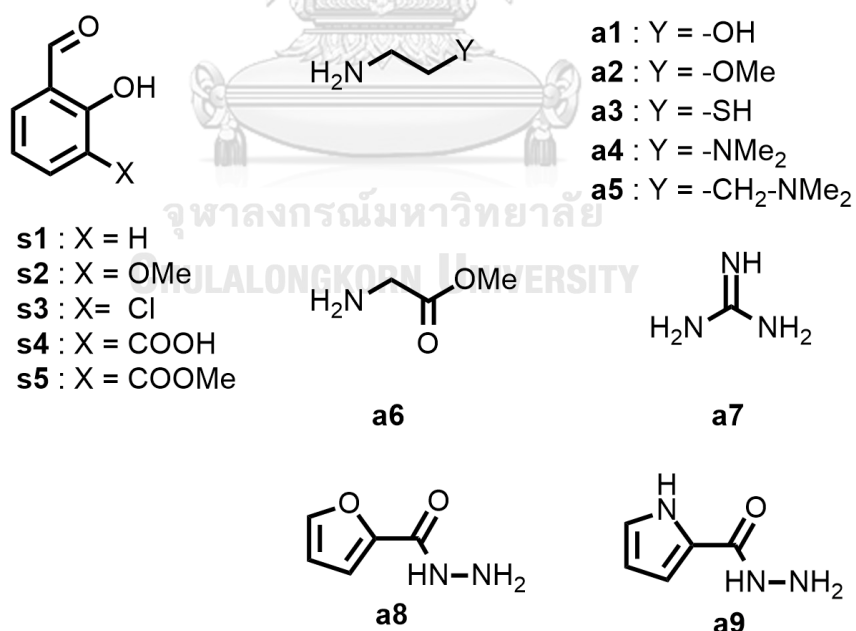
Methyl 3-formyl-2-hydroxybenzoate (**s5**) was successfully synthesized from esterification of commercially available 3-formyl-2-hydroxybenzoate (**s4**) in 83% yield. 2-pyrrolicarbohydrazide (**a9**) was synthesized from the condensation reaction between the methyl ester of pyrroic acid and hydrazine monohydrate in 29% overall yield (2 steps). (Scheme 3.1)



Scheme 3.1 Synthesis of **s5**, **a8** and **a9**.

3.2 Metal ion sensing test of salicylaldehydes

Aldehydes and amines are expected to readily condense to form the corresponding imines at room temperature. This allows synthesis and screening of imine chemosensors to be performed in a single step. In this work, 5 salicylaldehyde derivatives (**s1-s5**) and 9 amines (**a1-a9**) were used as the imine building blocks. (Scheme 3.2) This process would hypothetically yield 50 chemosensors, consisting 5 salicylaldehydes and 45 imines, that prompt a high throughput screening for metal ion sensors. These 50 chemosensors were tested with 18 metal ions (Li^+ , Na^+ , K^+ , Mg^{2+} , Ca^{2+} , Ba^{2+} , Al^{3+} , Fe^{2+} , Fe^{3+} , Cr^{3+} , Co^{2+} , Ni^{2+} , Cu^{2+} , Zn^{2+} , Ag^+ , Cd^{2+} , Hg^{2+} and Pb^{2+}) in comparison with Milli-Q water used as a blank. The photographic images of the mixture of aldehydes, amines and metal ions in methanol in 96 well-plate were recorded with a digital camera under black light (365 nm) to generate an array of 950 images ($5 \times 10 \times 19$) (Figure 3.1).



Scheme 3.2 Structures of salicylaldehydes and amines.

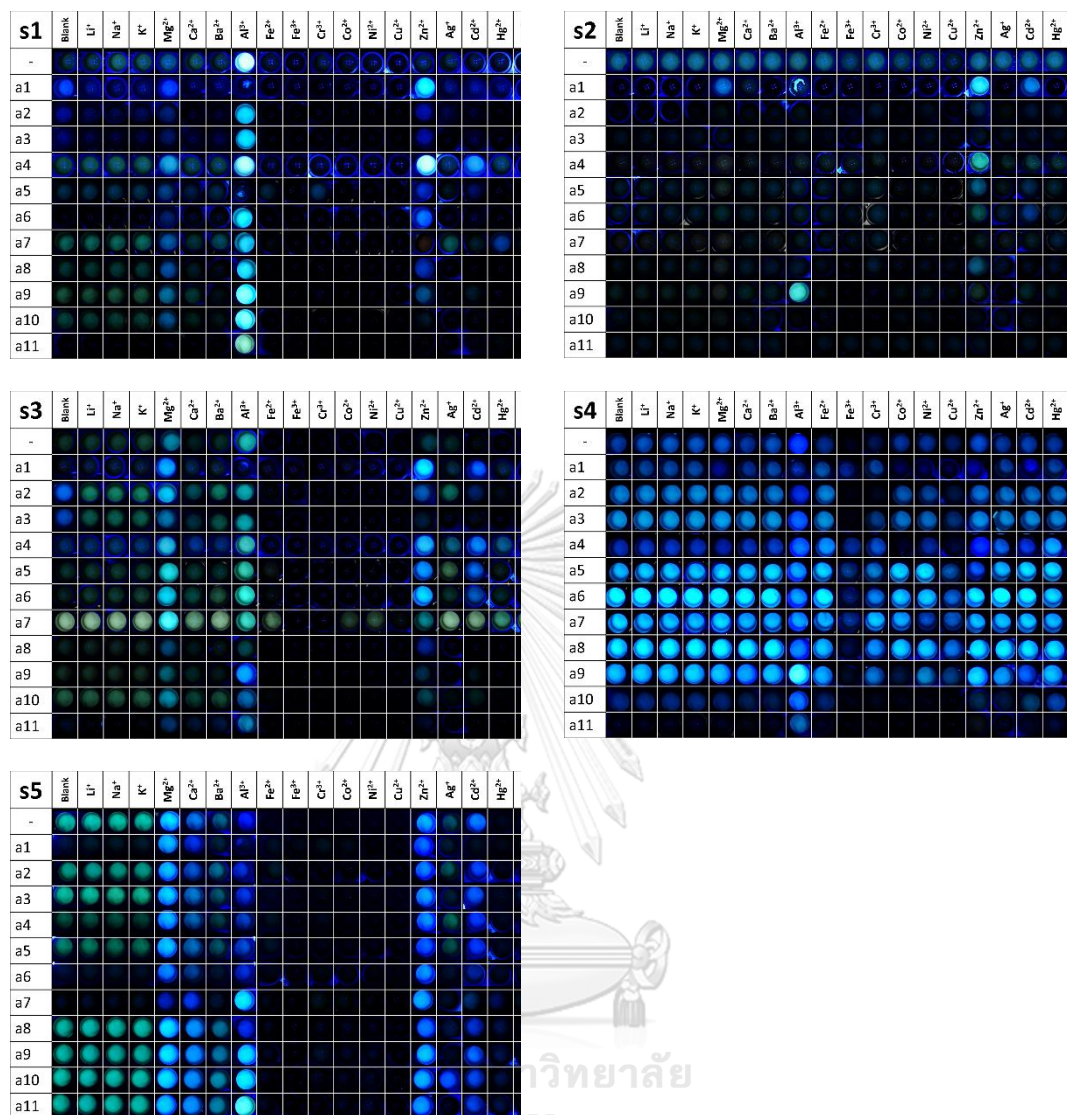


Figure 3.1 The photographic images of fluorescence responses of mixtures of salicylaldehydes (**s1-s5**, 1 mM) and amines (**a1-a9**, 1 mM) to metal ions (1 mM) under black light (365 nm).

From Figure 3.1, the salicylaldehydes themselves give some fluorescence responses to metal ions and several hypothetical imines have responses different from the corresponding salicylaldehydes. The results implied *in-situ* formation of the imines from the mixtures of aldehydes and amines. To confirm the *in-situ* formation of the imine, the NMR spectrum of a mixture of an equimolar of **s2** and **a4** in CDCl₃ was acquired after a few minutes of mixing. The ¹H NMR spectrum confirmed that the imine **s2a4** was rapidly formed and the imine product could be isolated (Figure 3.2).

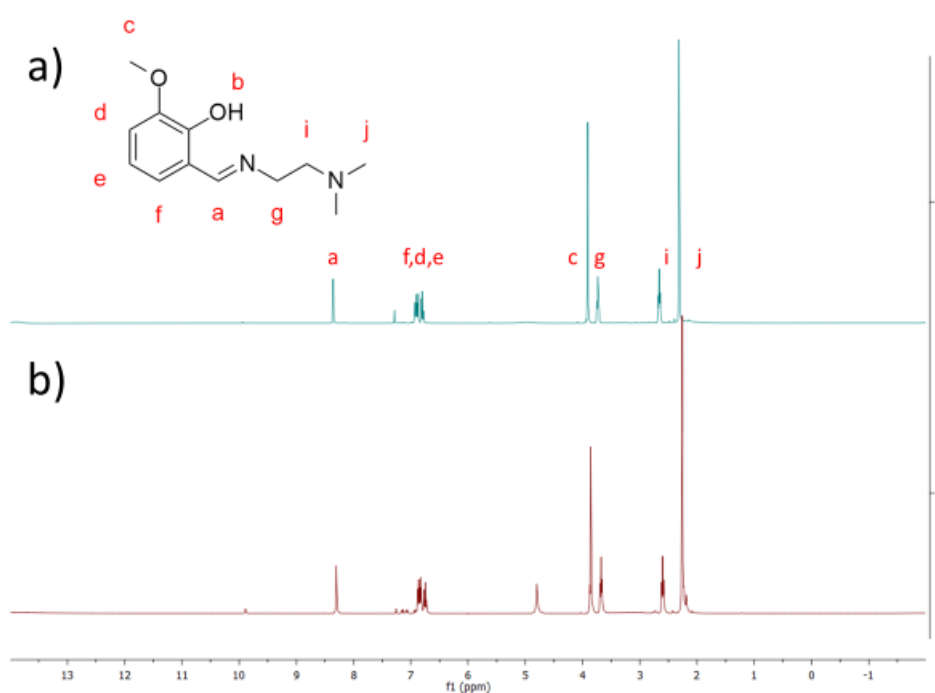


Figure 3.2 ¹H NMR of a) mixture of 1:1 mole ratio of **s2** and **a4**, b) isolated **s2a4**

The photographic images (Figure 3.1) also demonstrate that each metal ion create different pattern of fluorescence responses on the salicylaldehydes and imines. With application of pattern recognition process, these patterns should be useful for metal ion identification, that will be described in detail in the next section.

The imine **s2a4** was tested for metal ions selectivity with various metal ions (Li⁺, Na⁺, K⁺, Mg²⁺, Ca²⁺, Ba²⁺, Al³⁺, Fe²⁺, Fe³⁺, Cr³⁺, Co²⁺, Ni²⁺, Cu²⁺, Zn²⁺, Ag⁺, Cd²⁺, Hg²⁺ and Pb²⁺). It showed high selectivity toward Zn²⁺ in methanolic solution, corresponding

to the screening results. (Figure 3.3) Besides Zn^{2+} , Al^{3+} and Cd^{2+} could moderately enhance the fluorescence intensity of **s2a4**.

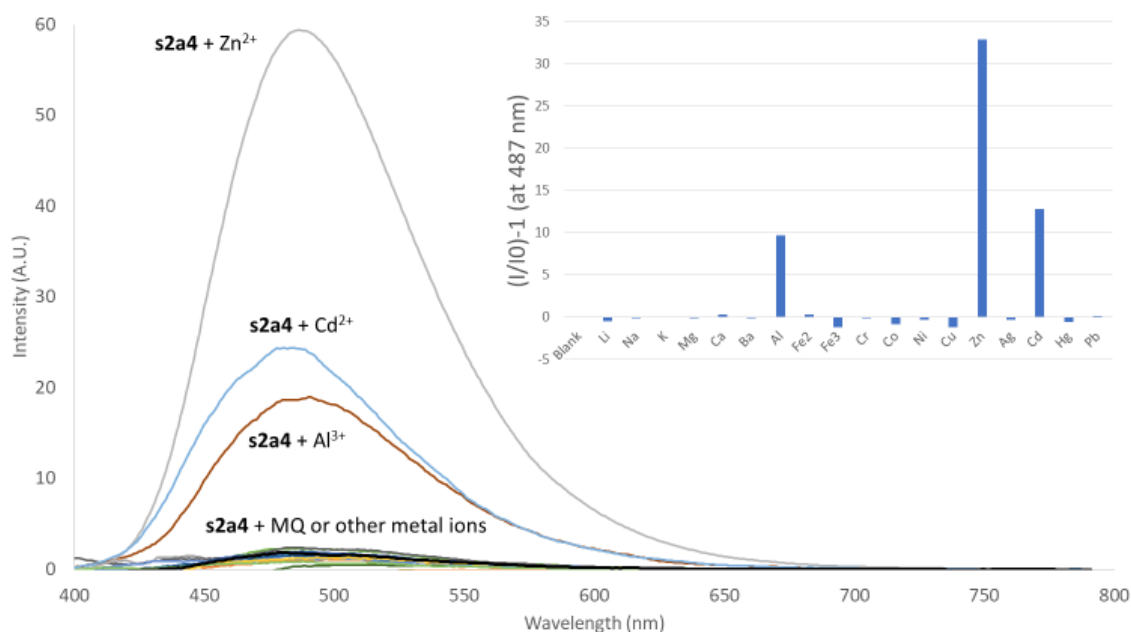


Figure 3.3 Fluorescence spectra of 10 μM of **s2a4** in the presence of various metal ions (100 μM) in MeOH:water (999:1) using $\lambda_{\text{ex}} = 375 \text{ nm}$.

3.3 Multivariate statistical analysis

To analyze the pattern of the fluorescence responses, the photographic images were converted into R, G and B values and analyzed by principal components analysis (PCA) to determine an appropriate set of sensing elements in a chemosensor array for metal ions identification. The fluorescence responses were represented by the color differences (ΔR , ΔG and ΔB) between the images of the mixtures with and without the metal ions. As the alkaline metals induce very minimal fluorescence responses to all sensors, the data related to these metal ions were discarded, leaving 800 images (5 x 10 x 16) for further analysis. Thus, the total of 2,400 ΔR , ΔG and ΔB values (3 x 800) were used as input to PCA analysis. The loadings of ΔR , ΔG and ΔB values in the first 3 principal components (PCs) of each sensor were combined, normalized and plotted as shown in Figure 3.4. The plot shows that imines of **s2** give low loading values in

correspondence to their low fluorescence responses, while many imines of **s1**, **s4** and **s5** have high loading values that are in good agreement with their distinct fluorescence responses to different metal ions. Therefore, these combined loadings approximately represent the contribution of each sensors to the pattern of the fluorescence responses generated by each metal ion. The combined loadings may be used as a criterion in the selection of sensor candidates for the metal ion identifying array.



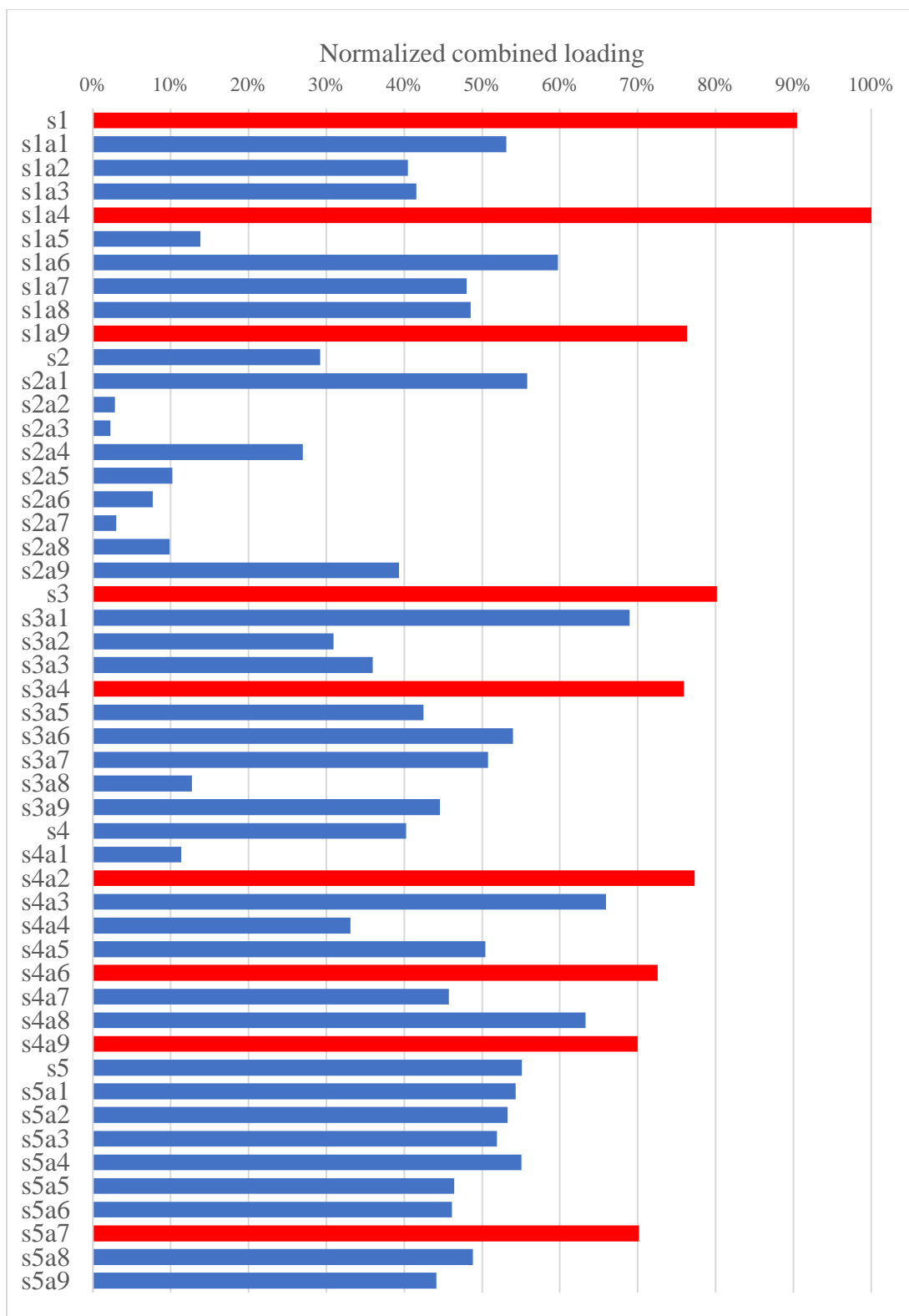


Figure 3.4 Bar chart of combined loading values of ΔR , ΔG and ΔB values in the first 3 PCs of each sensor normalized to 100% for the maximum values. Red bars indicate selected imines.

In practice, an array with lower number of sensors is more convenient to be used in metal ion analysis. To reduce the numbers of sensors candidates for metal ion identification, 9 sensors (red bar in Figure 3.5: **s1, s1a4, s1a9, s3, s3a4, s4a2, s4a6, s4a9 and s5a7**) in which each sensor has the normalized combined loading of 70% or above were selected. The selected imines were tested with 15 metal ions and blank for 10 repetitions to generate 1,440 fluorescence response images (9 sensors x 16 analytes x 10 repetitions), which produced 4,320 ΔR , ΔG and ΔB values. The PCA-score plot of ΔRGB inputs in the first 3 PCs, containing 91.79% of variance, showed 16 clusters of scores corresponding to 16 analytes (Figure 3.5). The score clusters of Al^{3+} , Zn^{2+} , Cd^{2+} , Mg^{2+} and Fe^{3+} are well-separated, in consistent with the distinct fluorescence response patterns in the photographic images (Figure 3.1). On the other hand, the clusters of Milli-Q water (blank), Ca^{2+} and Ba^{2+} are quite close with some overlap that suggest weak interaction between these metal ions and the sensors.

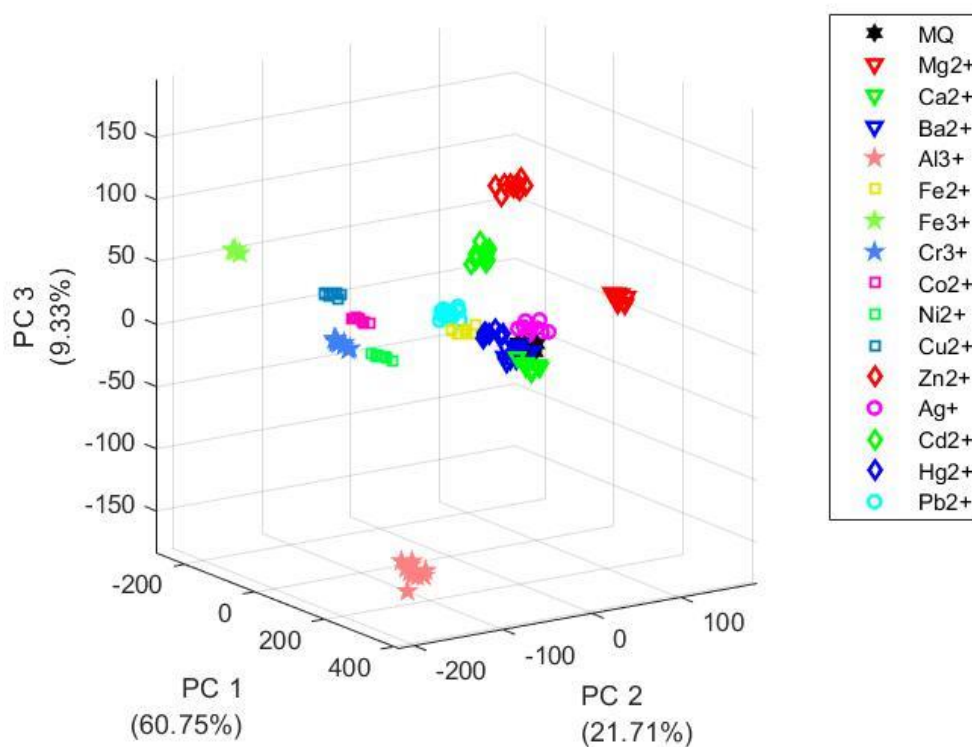


Figure 3.5 PCA score plot of ΔR , ΔG and ΔB values from 9 selected sensors tested with 15 metal ions and Mili-Q water.

The classification of metal ions based on PCA scores was subjected to Linear Discrimination Analysis Leave-Out-Out Cross Validation (LDA-LOOCV), and 158 out of 160 data points were correctly classified with only 2 points of Ba^{2+} were misclassified as Milli-Q water.

To minimize number of imines required in discrimination of metal ions, ΔRGB from 9 sensors were grouped in all possible combinations from 1-9 sensors, to provide a total of 511 combinations. The ΔRGB values in these combinations were converted into scores by PCA. The scores were again subjected to LDA-LOOCV to determine the classification accuracy of each combination. A plot of the accuracy values is presented in Figure 3.6 which shows that the accuracy reach saturation with the combination of at least 2 sensors. Among 36 combinations of 2 sensors, the **s4a9** and **s5a7** pair gave the highest accuracy of 99%.

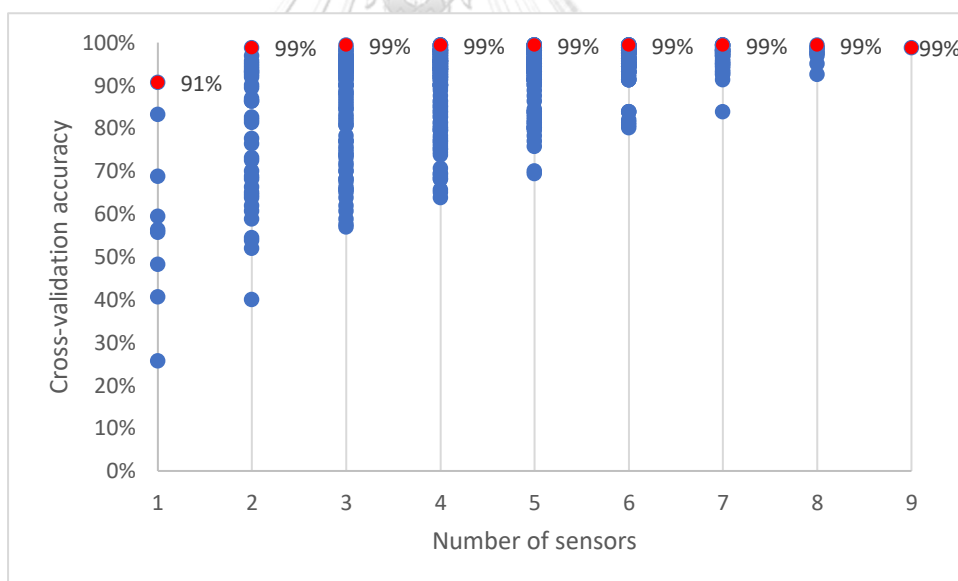


Figure 3.6 Plot of classification accuracy derived from LOOCV when using possible combinations of 1-9 sensors.

The PCA score plot of ΔRGB from **s4a9** and **s5a7** showed that all 3 PCs contained satisfying 98.25% of variance and the cross-validation gave only 2 misclassified samples out of 160 samples, representing an accuracy of 99% (Figure 3.7). The misclassified samples are Ba^{2+} and Hg^{2+} ions, which were classified as Mili-Q water.

Therefore, the reduction of number of sensors in the array to 2 sensing compounds gave satisfying results.

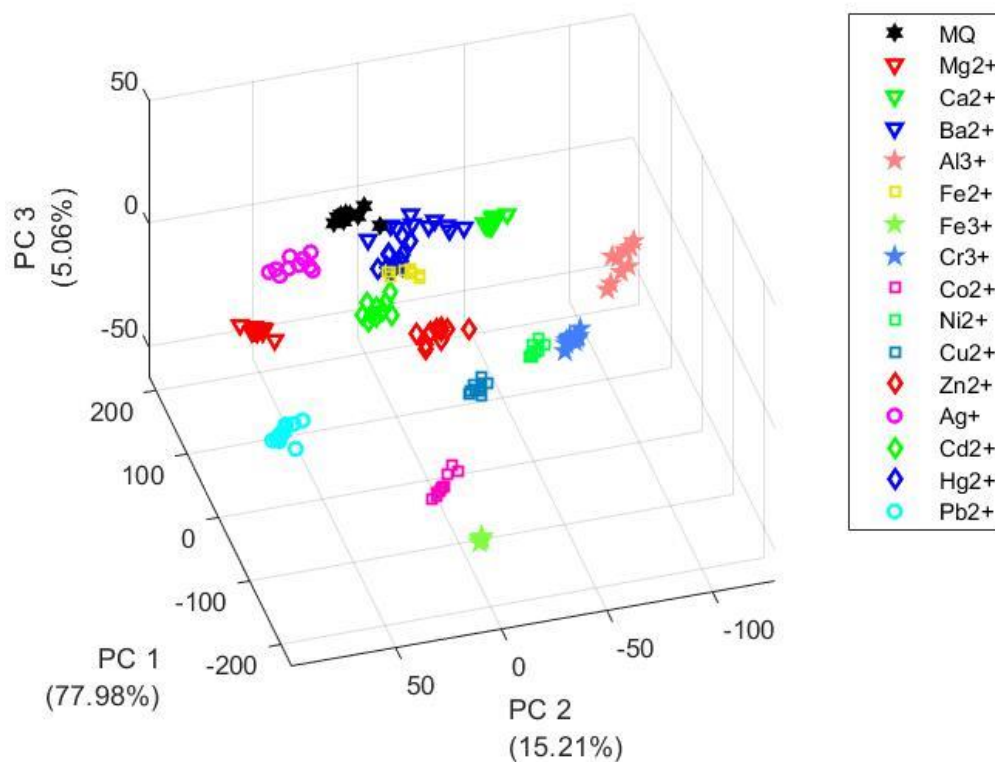
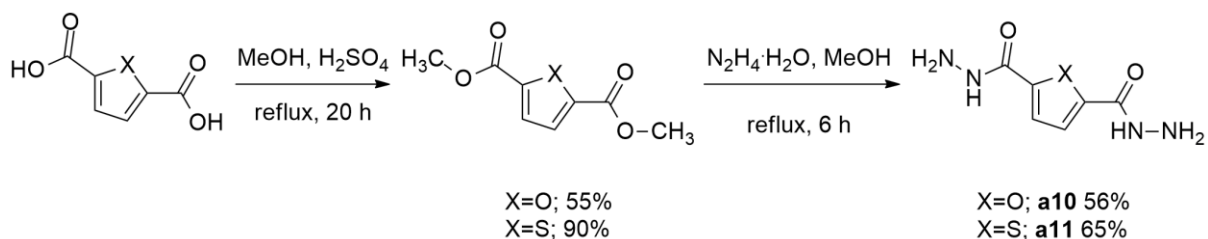


Figure 3.7 PCA score plot of Δ RGB values from s4a9 and s5a7.

3.4 Study of dihydrazide sensors

In addition of 9 amines, 2 dihydrazides derivatives were synthesized and tested with metal ions. Furan-2,5-dicarbohydrazide (**a10**) and thiophene-2,5-dicarbohydrazide (**a11**) were successfully synthesized from the condensation reaction between hydrazine monohydrate and methyl ester of furan-2,5-dicarboxylic diacid or thiophene-2,5-dicarboxylic diacid, respectively. The overall yield was 31% for **a10** and 65% for **a11** (Scheme 3.2).



Scheme 3.3 Synthesis of **a10** and **a11**.

With two additional dihydrazides **a10** and **a11**, it was possible to screen for new metal ion sensors based on *in situ* condensation between the dihydrazides and salicylaldehydes similar to the method described in section 3.2. Stock solution of both dihydrazides **a10** and **a11** in DMSO were mixed with each of salicylaldehydes (**s1-s5**) in methanol in the presence of various metal ions. The photographic images of the fluorescence responses recorded under 365 nm UV lamps showed that both **s1a10** and **s1a11** are highly selective with Al^{3+} ion (Figure 3.8). It is interesting to note that the color of the fluorescence images for **s1a11** in the presence of Al^{3+} is green while that of **s1** is blue (see Figure 3.8 and Figure 3.1 for comparison).

Hydrazones	Blank	Li^+	Na^+	K^+	Mg^{2+}	Ca^{2+}	Ba^{2+}	Al^{3+}	Fe^{2+}	Fe^{3+}	Cr^{3+}	Co^{2+}	Ni^{2+}	Cu^{2+}	Zn^{2+}	Ag^+	Cd^{2+}	Hg^{2+}	Pb^{2+}
s1a10								Blue											
s1a11								Green											
s2a10																			
s2a11																			
s3a10																			
s3a11																			
s4a10																			
s4a11																			
s5a10																			
s5a11																			

Figure 3.8 The photographic images of fluorescence responses of mixtures of salicylaldehydes (**s1-s5**, 1 mM) and amines (**a10** and **a11**, 1 mM) to metal ions (1 mM) under black light (365 nm).

The hydrazone **s1a11** was chosen for further investigation. It was isolated from the reaction between **s1** and **a11**. In the presence of Al^{3+} , the methanolic solution of

s1a11 exhibited longer maximum emission wavelength (λ_{em}) at 499 nm in comparison with **s1** (λ_{em} = 483 nm) (Figure 3.9). The results correspond to the longer π -conjugation of **s1a11** and are in good agreement with the color appeared in the photographic images.

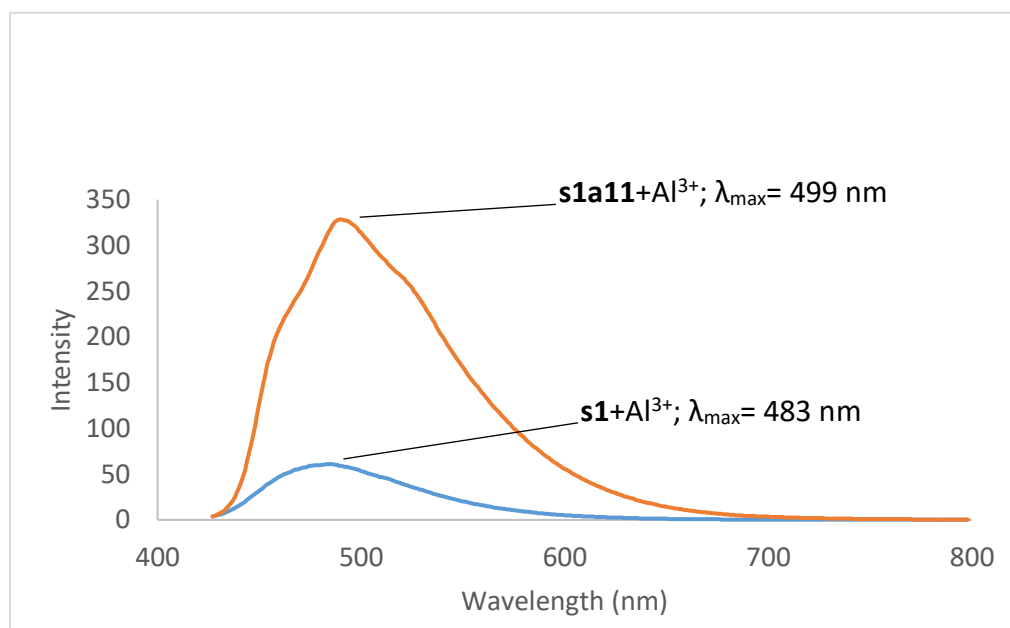


Figure 3.9 Fluorescence spectra of 10 μM of **s1** and **s1a11** in the presence of 100 μM Al^{3+} in MeOH:water (9:1) using λ_{ex} = 415 nm.

For metal ion selectivity test, the fluorescence spectra of **s1a11** in the presence of various metal ions (Li^+ , Na^+ , K^+ , Mg^{2+} , Ca^{2+} , Ba^{2+} , Al^{3+} , Fe^{2+} , Fe^{3+} , Cr^{3+} , Co^{2+} , Ni^{2+} , Cu^{2+} , Zn^{2+} , Ag^+ , Cd^{2+} , Hg^{2+} and Pb^{2+}) were acquired. When excited at 415 nm, **s1a11** exhibited selective fluorescence turn-on signal to Al^{3+} (Figure 3.10).

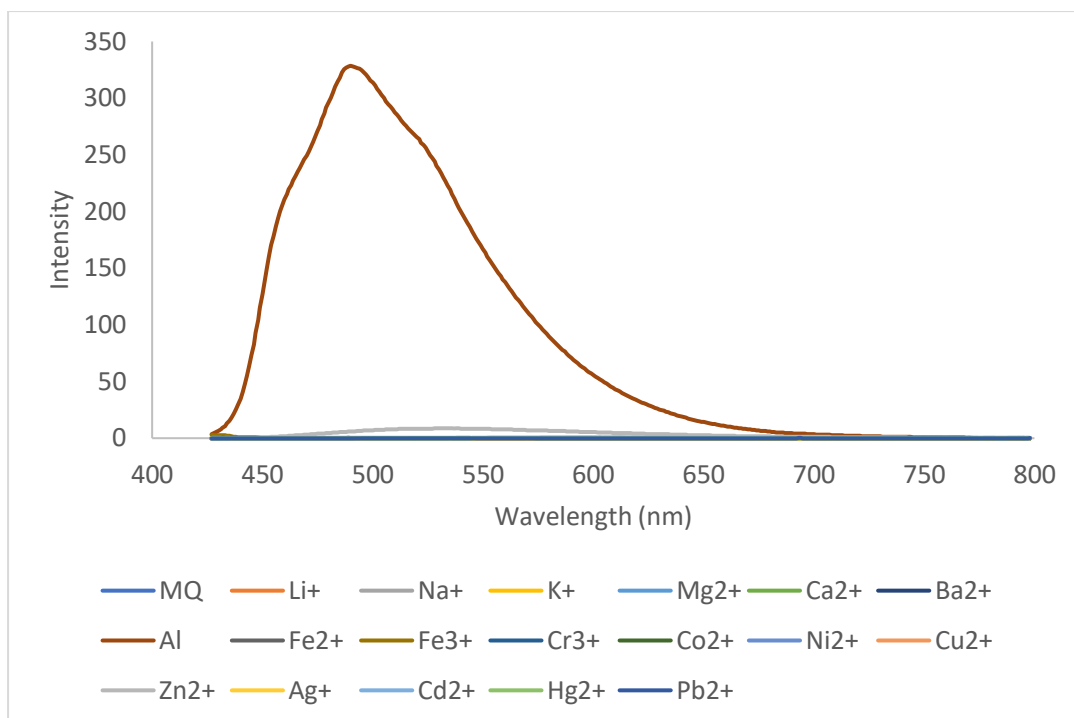


Figure 3.10 Fluorescence spectra of 10 μM of **s1a11** in the presence of various metal ions (100 μM) in MeOH:water (9:1) using $\lambda_{\text{ex}} = 415 \text{ nm}$.

Further investigation found that fluorescence response of **s1a11** with Al^{3+} was time-dependent (Figure 3.11). The fluorescence intensity increased more than 6-fold over course of an hour.

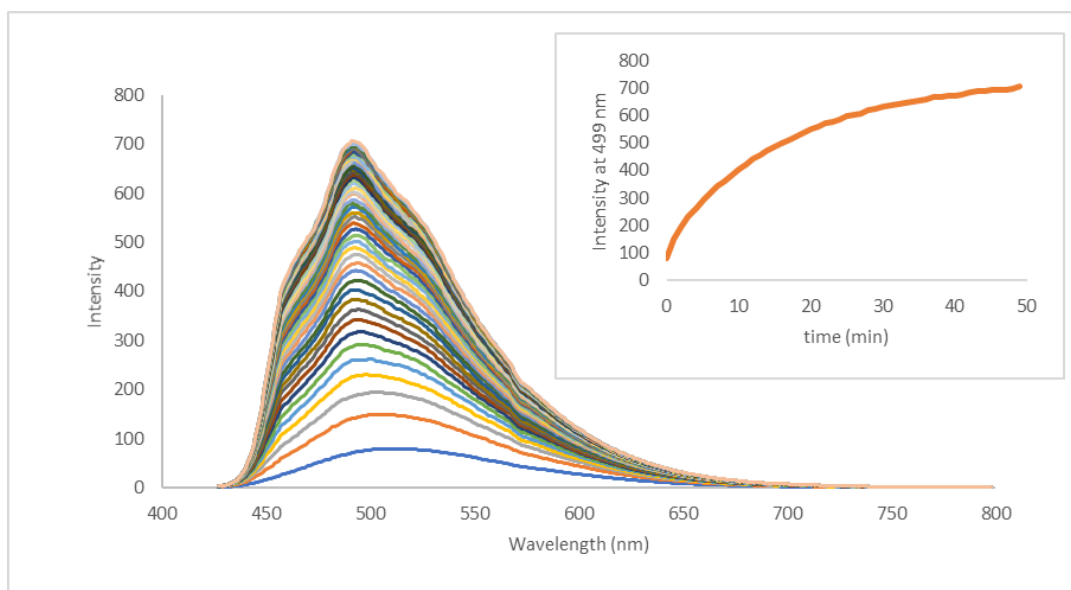


Figure 3.11 Time-dependent fluorescence intensity of **s1a11** with Al^{3+} ($\lambda_{\text{ex}} = 415 \text{ nm}$), inset: Fluorescence intensity at 499 nm over time.

The ^1H NMR spectrum of isolated **s1a11** showed 2 prominent sets of signals with an integral ratio of 0.65:0.35 (Figure 3.12). This may be due to *cis-trans* isomerization of the imine double bonds of the hydrazone [17]. The *trans* isomer allows an intramolecular hydrogen bonding between phenolic proton and imine nitrogen via a 6-membered ring while the intramolecular hydrogen bonding in the *cis* isomer form via a less stable 7-membered ring. Therefore, the *trans* isomer was probably the larger fraction (0.65) observed in the ^1H NMR spectrum. In fact, there could be 3 possible isomers of **s1a11** i.e. *trans-trans*, *trans-cis* and *cis-cis*. The isomerization between these forms can have thermodynamic and kinetic effects on the complexation between **s1a11** and Al^{3+} .

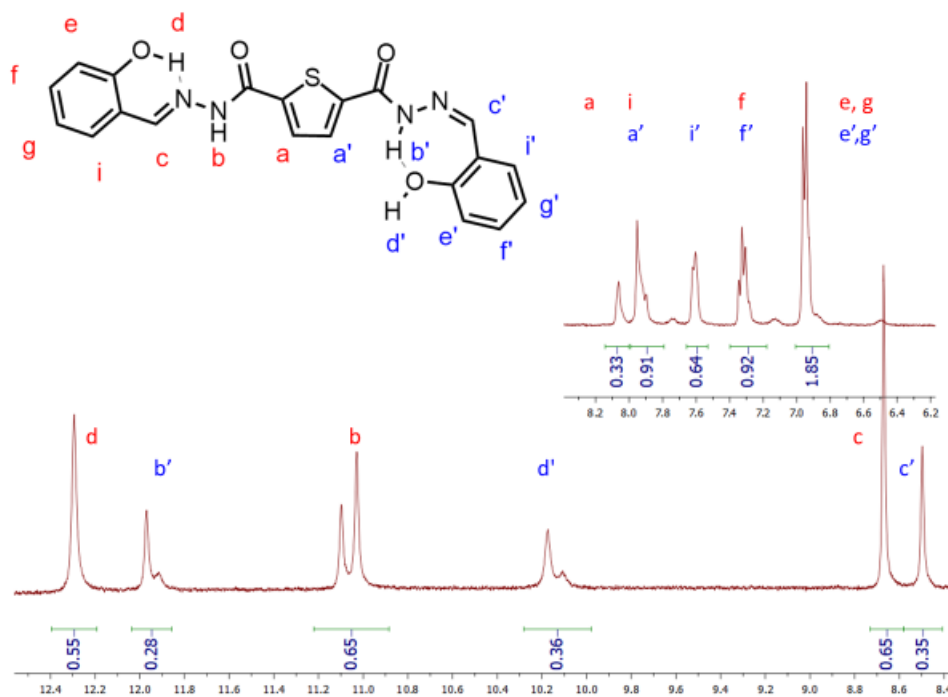


Figure 3.12 ^1H NMR spectrum of **s1a11** in DMSO-d_6 .

NMR titration between **s1a11** and Al^{3+} up to 2 equivalents (Figure 3.13) showed a new set of signals at 12.21, 11.87, 11.03, 8.54, 8.00, 7.69, 7.38 and 6.69 ppm. This result suggested that **s1a11** formed complex with Al^{3+} , but even with 2 equivalents of Al^{3+} and more than 24 hours, some of the signals of non-complexed **s1a11** remained. The sensing mechanism of this compound cannot be concluded and require further investigation

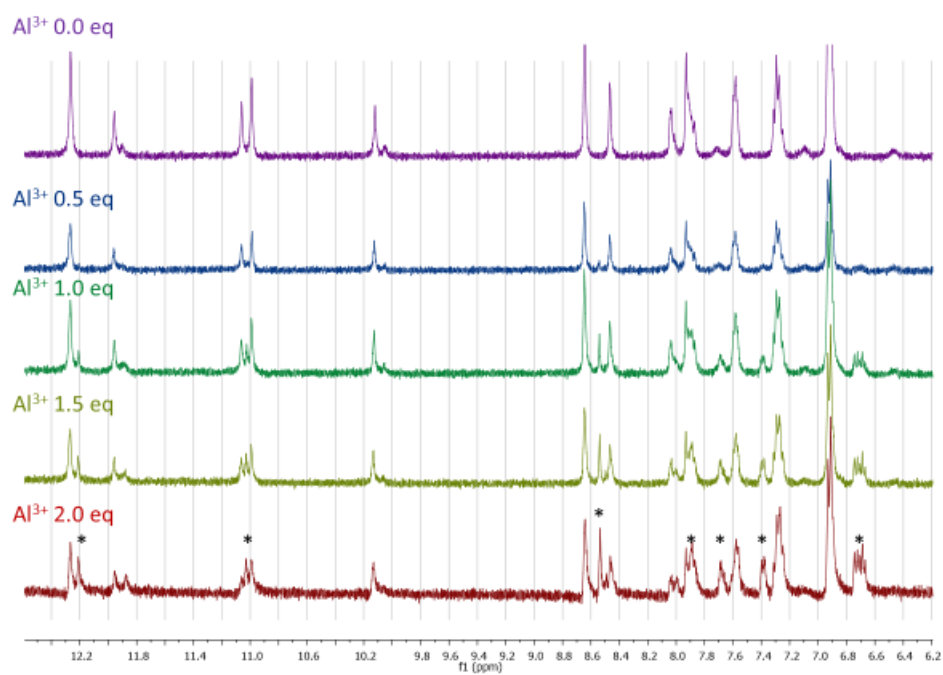


Figure 3.13 ^1H NMR titration of s1a11 and $\text{Al}_2(\text{SO}_4)_3$ in DMSO.



CHAPTER IV

CONCLUSION

A set of 50 fluorescent chemosensors including 5 salicylaldehydes and their 45 imines, generated in-situ from the aldehydes-amine condensation, were simultaneously screened with 18 metal ions in 96-well plates under black light. The principal components analysis (PCA) of the Δ RGB values obtained from the photographic images in the screening process showed 9 sensors with normalized loading value over 70%. The sensor array constructed from these 9 sensors could classify 10 solutions containing each of 15 non-alkali metal ions with 99% accuracy from a leave-one-out cross-validation. The cross-validation of full factorial combinations of the sensors from 2 to 9 identified the combinations of 2 sensors could also classify the metal ions without any loss of accuracy. Using this rapid in-situ forming-screening technique, a new sensor selective to Al^{3+} was easily identified from 10 hydrazones generated from 5 salicylaldehyde and 2 dihydrazides. However, the response time of the hydrazine sensor was relatively slow that related to reaction mode of sensing which require further investigation.



APPENDIX

จุฬาลงกรณ์มหาวิทยาลัย
CHULALONGKORN UNIVERSITY

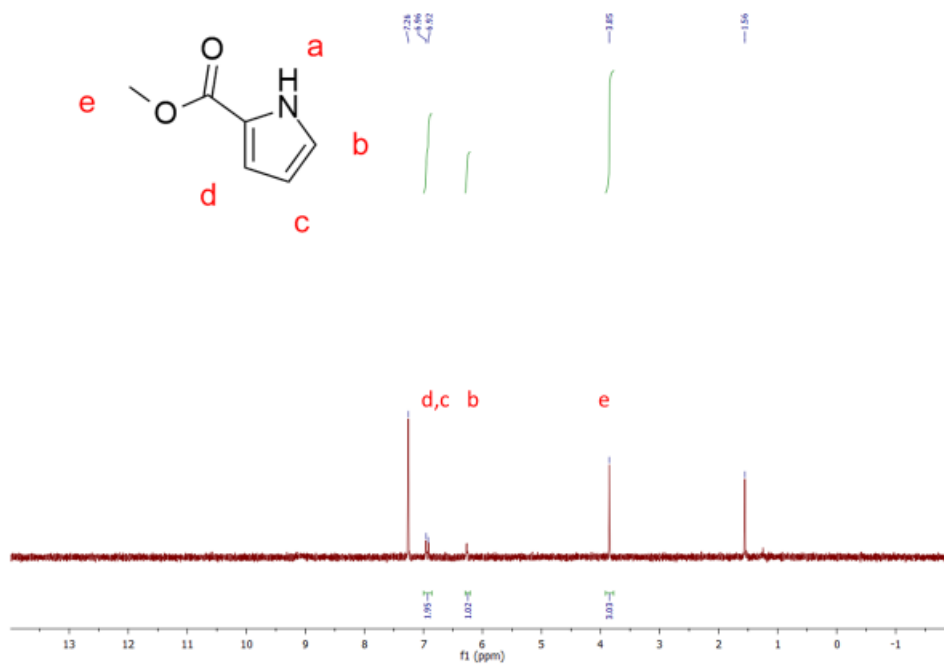


Figure A 1 ^1H NMR spectrum of Methyl 2-pyrrolicarboxylate in CDCl_3 .

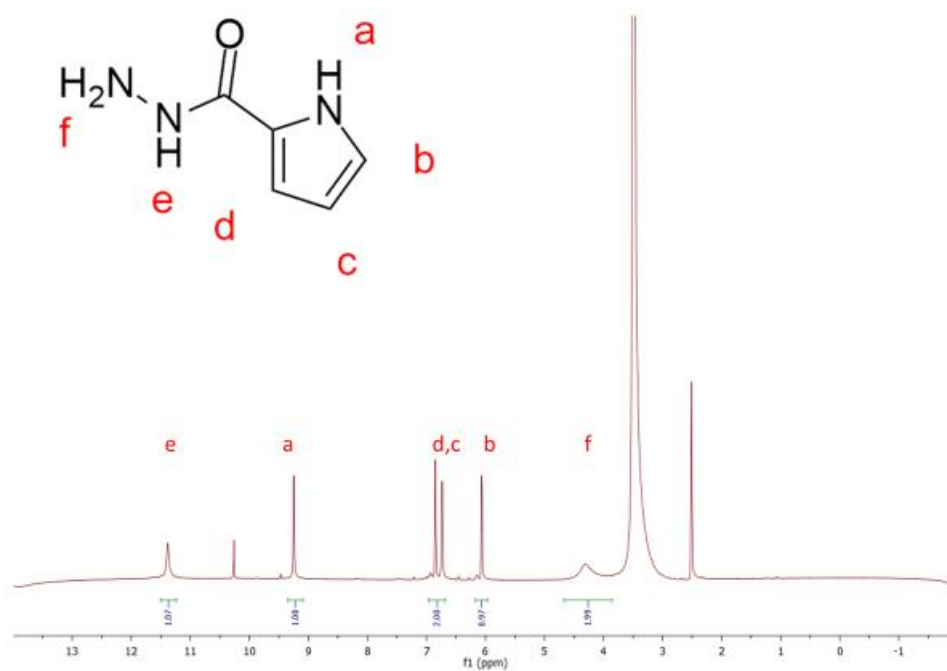


Figure A 2 ^1H NMR spectrum of compound **a9** in DMSO-d_6 .

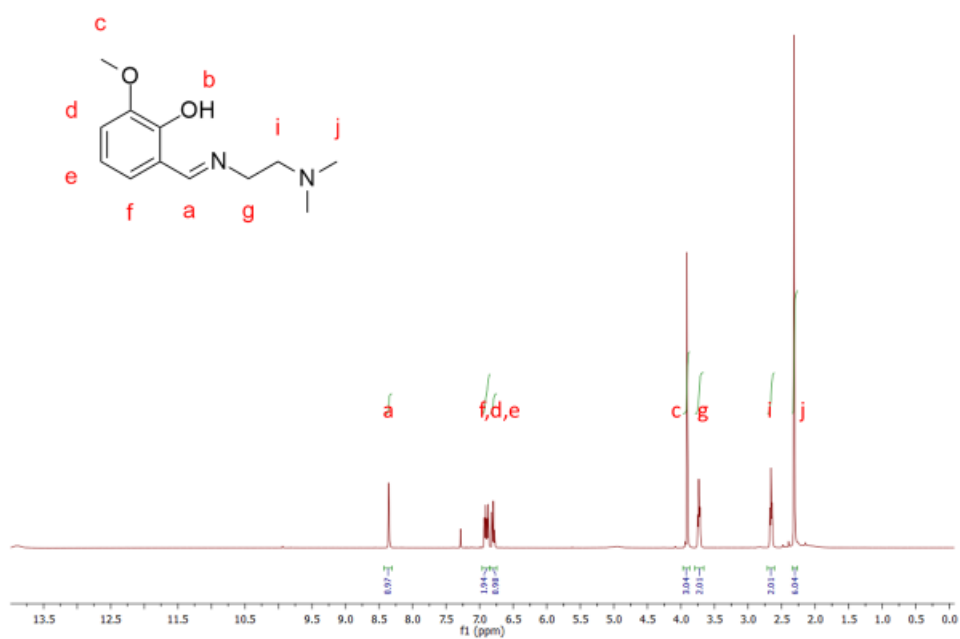


Figure A 3 ^1H NMR spectrum of compound **s2a4** in CDCl_3 .

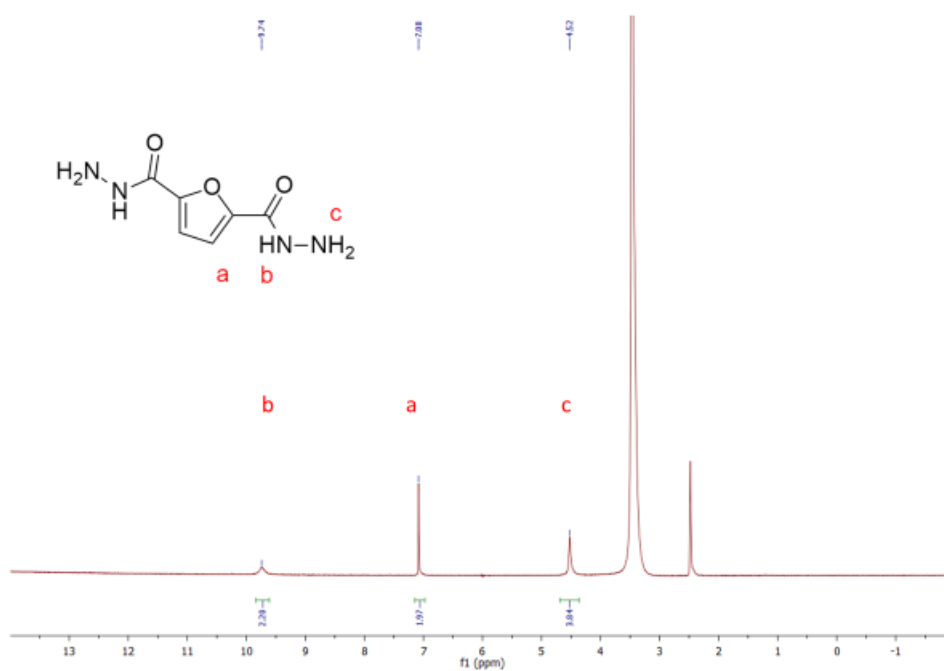


Figure A 4 ^1H NMR spectrum of compound **a10** in DMSO-d_6 .

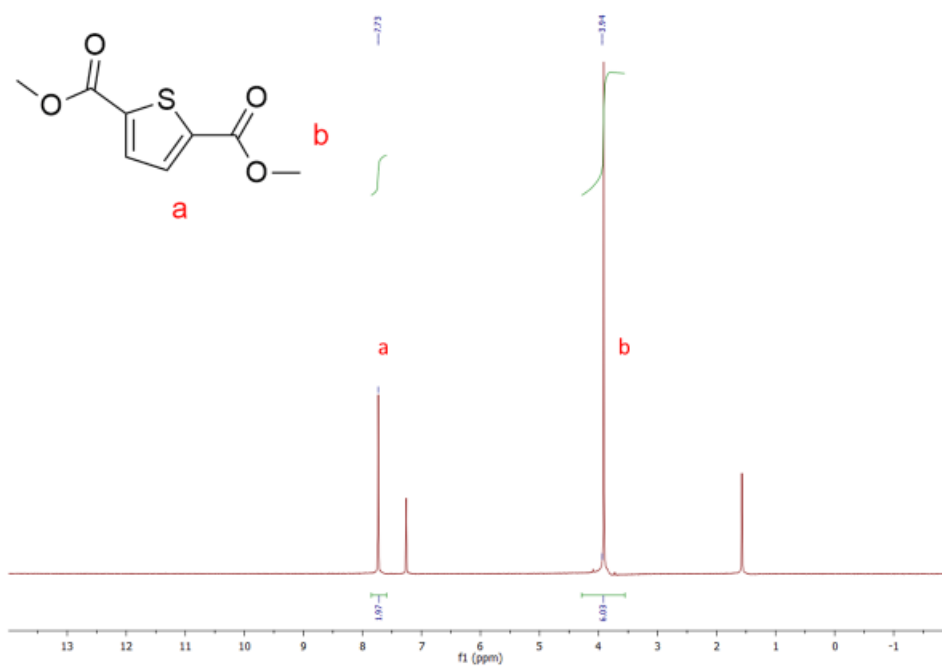


Figure A 5 ¹H NMR spectrum of compound **s2a4** in CDCl₃

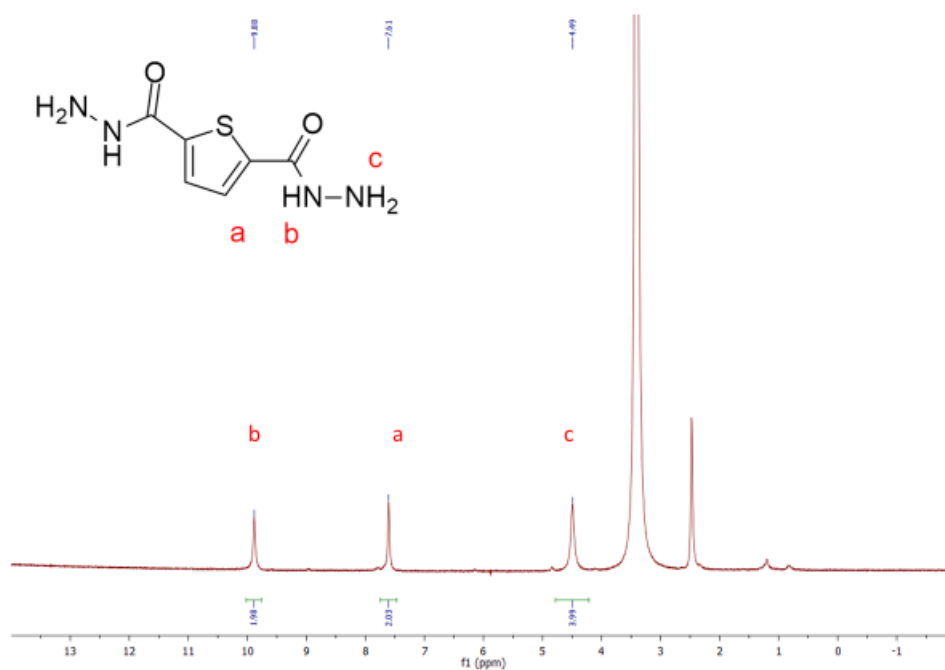


Figure A 6 ¹H NMR spectrum of compound **a11** in DMSO-d₆.

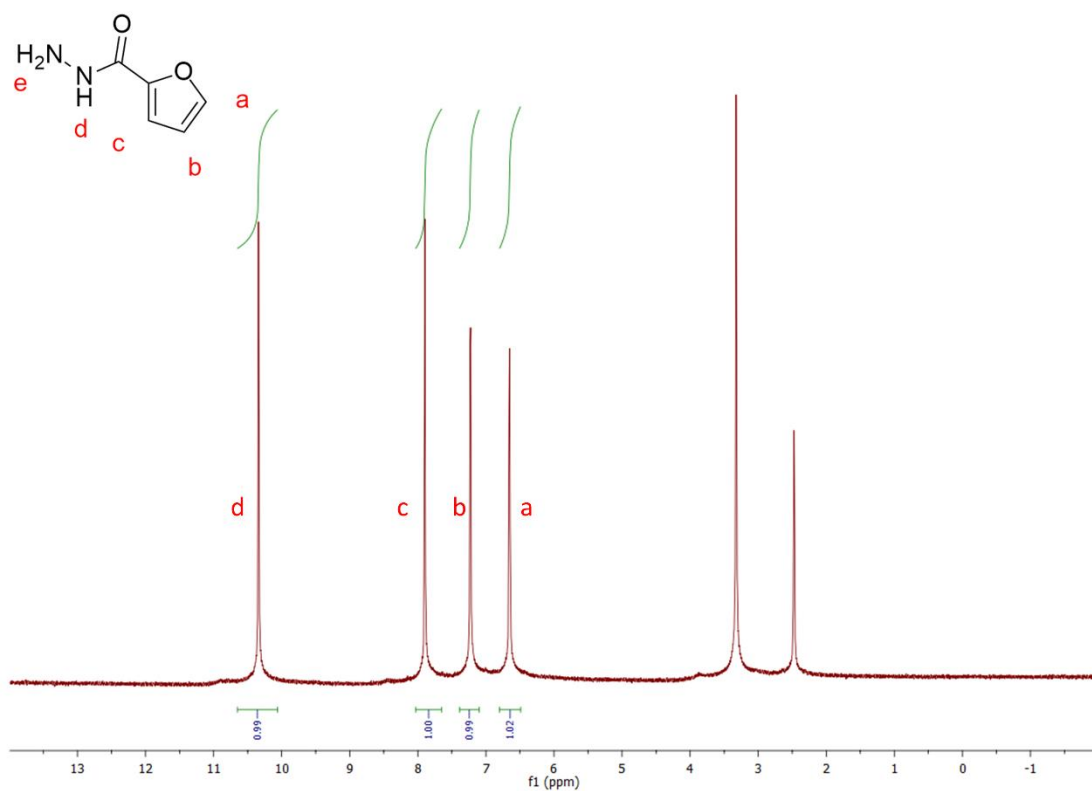


Figure A 7 ^1H NMR spectrum of compound **a8** in DMSO-d_6

REFERENCES

1. Environmental_Protection_Agency, National Primary Drinking Water Regulations. Environmental Protection Agency: 2009; pp <https://www.epa.gov/ground-water-and-drinking-water/national-primary-drinking-water-regulations>.
2. World_Health_Organization, *Vitamin and mineral requirements in human nutrition*. 2 ed.; World Health Organization: <https://apps.who.int/iris/handle/10665/42716>, 2005.
3. Lakowicz, J. R., *Principles of Fluorescence Spectroscopy*. 3 ed.; Springer science & Business media: New York, 2006.
4. Chen, C.-H.; Liao, D.-J.; Wan, C.-F.; Wu, A.-T., A turn-on and reversible Schiff base fluorescence sensor for Al³⁺ ion. *Analyst* **2013**, *138*, 2527-2530.
5. Chen, K.-Y.; Tsai, H.-Y., Synthesis, X-ray Structure, Spectroscopic Properties and DFT Studies of a Novel Schiff Base. *Int. J. Mol. Sci.* **2014**, *15*, 18706-18724.
6. Pradhan, A. B.; Mandal, S. K.; Banerjee, S.; Mukherjee, A.; Das, S.; Khuda Bukhsh, A. R.; Saha, A., A highly selective fluorescent sensor for zinc ion based on quinoline platform with potential applications for cell imaging studies. *Polyhedron* **2015**, *94*, 75-82.
7. Sarkar, D.; Pramanik, A.; Jana, S.; Karmakar, P.; Mondal, T. K., Quinoline based reversible fluorescent 'turn-on' chemosensor for the selective detection of Zn²⁺: Application in living cell imaging and as INHIBIT logic gate. *Sens. Actuators, B* **2015**, *209*, 138-146.
8. Saleh, S. M.; Ali, R.; Elshaarawy, R. F. M., A ratiometric and selective fluorescent chemosensor for Ca(ii) ions based on a novel water-soluble ionic Schiff-base. *RSC Adv.* **2016**, *6*, 68709-68718.
9. Boonkitpatarakul, K.; Wang, J.; Niamnont, N.; Liu, B.; McDonald, L.; Pang, Y.; Sukwattanasinitt, M., Novel Turn-On Fluorescent Sensors with Mega Stokes Shifts for Dual Detection of Al³⁺ and Zn²⁺. *ACS Sens.* **2016**, *1*, 144-150.
10. Potyrailo, R. A.; Mirsky, V. M., *Combinatorial Methods for Chemical and Biological Sensors*. GE Global Research Center: Niskayuna, NY, 2009.

11. Mello, J. V.; Finney, N. S., Reversing the Discovery Paradigm: A New Approach to the Combinatorial Discovery of Fluorescent Chemosensors. *J. Am. Chem. Soc.* **2005**, *127*, 10124-10125.
12. Yuen, L. H.; Franzini, R. M.; Tan, S. S.; Kool, E. T., Large-Scale Detection of Metals with a Small Set of Fluorescent DNA-Like Chemosensors. *J. Am. Chem. Soc.* **2014**, *136*, 14576-14582.
13. Kovaříček, P.; Meister, A. C.; Flídrová, K.; Cabot, R.; Kovaříčková, K.; Lehn, J. M., Competition-driven selection in covalent dynamic networks and implementation in organic reactional selectivity. *Chemical Science* **2016**, *7*, 3215-3226.
14. Palacios, M. A.; Wang, Z.; Montes, V. A.; Zyryanov, G. V.; Anzenbacher, P., Rational Design of a Minimal Size Sensor Array for Metal Ion Detection. *J. Am. Chem. Soc.* **2008**, *130*, 10307-10314.
15. Wang, Z.; Palacios, M. A.; Anzenbacher, P., Fluorescence Sensor Array for Metal Ion Detection Based on Various Coordination Chemistries: General Performance and Potential Application. *Anal. Chem.* **2008**, *80*, 7451-7459.
16. Mungkarndee, R.; Tumcharern, G.; Thiramanus, R.; Techakriengkrai, I.; Sukwattanasinitt, M., Fluorescence sensor arrays for identification of foodborne pathogens. *Anal. Methods* **2015**, *7*, 7431-7435.
17. Cordier, C.; Vauthier, E.; Adenier, A.; Lu, Y.; Massat, A.; Cossé-Barbi, A., Salicylaldehyde Benzoyl Hydrazone: Isomerization Due to Water. A Structural Analysis Using a Combination of NMR, IR, and Theoretical Investigations. *Struct. Chem.* **2004**, *15*, 295-307.



จุฬาลงกรณ์มหาวิทยาลัย
CHULALONGKORN UNIVERSITY

VITA

NAME Phoom Sangsuwan

DATE OF BIRTH 18 June 1993

PLACE OF BIRTH Hadyai, Songkhla, Thailand

INSTITUTIONS ATTENDED Department of Chemistry, Faculty of Science,
Chulalongkorn University,
Phayathai Road, Pathumwan, Bangkok 10330, Thailand

HOME ADDRESS 249 Phetchakasem Rd.
Hadyai, Songkhla, Thailand 90110

